

1
2
3
4
5
6
7
8
9
10
11
12
13
14
15
16
17
18
19
20
21
22

**NEURONS THAT FUNCTION WITHIN AN INTEGRATOR TO PROMOTE A
PERSISTENT BEHAVIORAL STATE IN *DROSOPHILA***

Yonil Jung¹, Ann Kennedy¹, Hui Chiu¹, Farhan Mohammad^{2,3,4}, Adam Claridge-Chang^{2,3} and
David J. Anderson¹

Division of Biology 156-29
Howard Hughes Medical Institute
TianQiao and Chrissy Chen Institute for Neuroscience
California Institute of Technology
Pasadena, CA 91125¹

Neuroscience & Behavioural Disorders Programme
Duke-NUS Medical School
Singapore, 138673²
Institute of Molecular and Cell Biology
Singapore, 138673³

College of Health & Life Sciences
Hamad Bin Khalifa University
Doha, Qatar⁴

23 **SUMMARY**

24 **Innate behaviors involve both reflexive motor programs and internal states. In**
25 ***Drosophila*, optogenetic activation of male-specific P1 interneurons triggers courtship song,**
26 **as well as a persistent behavioral state that prolongs courtship and enhances aggressiveness.**
27 **Here we identify pCd neurons as persistently activated by repeated P1 stimulation. pCd**
28 **neurons are required for P1-evoked persistent courtship and aggression, as well as for**
29 **normal social behavior. Activation of pCd neurons alone is inefficacious, but enhances and**
30 **prolongs courtship or aggression promoted by female cues. Transient female exposure**
31 **induced persistent increases in male aggressiveness, an effect suppressed by transiently**
32 **silencing pCd neurons. Transient silencing of pCd also disrupted P1-induced persistent**
33 **physiological activity, implying a requisite role in persistence. Finally, P1 activation of pCd**
34 **neurons enhanced their responsiveness to cVA, an aggression-promoting pheromone. Thus,**
35 **pCd neurons function within a circuit that integrates P1 input, to promote a persistent**
36 **internal state that enhances multiple social behaviors.**

37 **INTRODUCTION**

38 Animal behaviors triggered by specific sensory cues evolve over multiple time-scales, from
39 rapid reflex reactions to more enduring responses accompanied by changes in internal state^{1,2}. The
40 former allow survival reactions, while the latter afford time to integrate contextual and other
41 influences on behavioral decisions. In *Drosophila melanogaster*, male-specific P1 interneurons³
42 are activated by female-specific pheromones⁴⁻⁶, and control male courtship behaviors such as
43 singing^{7,8}, as well as internal states that regulate aggression⁹, mating^{10,11}, feeding¹² and sleep¹³
44 (reviewed in Ref. ¹⁴). Artificial stimulation of P1 neurons in solitary males can trigger rapid-onset

45 courtship song^{7,8,15}. Nevertheless, singing persists for minutes after stimulation offset^{15,16}, while
46 optogenetically evoked P1 activity itself returns to baseline in tens of seconds^{9,15} (but see ref¹⁷).
47 Similarly, the effect of P1 activation to promote aggressiveness endures for minutes after
48 photostimulation offset¹⁸. These data suggest that persistent behavioral states evoked by P1
49 stimulation are not encoded in P1 neurons themselves, but rather in one or more of their
50 downstream targets. We therefore sought to identify such targets, and to understand their
51 functional role in the encoding of persistent behavioral states.

52 **RESULTS**

53 To search for P1 follower cells exhibiting persistent responses, we expressed the red-shifted
54 opsin Chrimson¹⁹ in P1^a-split GAL4 neurons^{9,18,20}, and a calcium indicator (GCaMP6s²¹) in ~2,000
55 Fruitless (Fru)-LexA²² neurons (Fig. 1a). Optogenetic stimulation was calibrated to activate P1
56 cells at a level comparable to that evoked in these cells by female abdomen touching in the same
57 preparation. Fru⁺ cells activated by P1 stimulation were identified by volumetric imaging (30 4-
58 μm optical sections covering a 250 μm x 250 μm x 120 μm volume; Extended Data Fig. 1 d, e).
59 On average, we monitored activity of 191 Fru⁺ cell somata and identified ~37 cells per fly that
60 responded to P1 stimulation ($\geq 2/3$ trials evoking a peak $\Delta F/F$ response $>4\sigma$ above baseline; ED
61 Fig. 1f), in 14 distinct brain regions. Different putative P1 follower cells showed different response
62 durations, in a continuous distribution ranging from those similar to P1 ($\tau \sim 15$ s; see Methods) to
63 those lasting much longer (Fig. 1b, ED Fig. 1g, i). We used several criteria to select cells for further
64 study: 1) median tau value > 5 -fold that of P1 ($\tau \sim 75$ s); 2) persistent P1 responses detected in
65 $>75\%$ of tested flies (n=12); 3) >2 cells/fly per hemibrain; 4) cells genetically accessible using
66 specific GAL4 drivers.

67 We identified several putative persistent P1 follower (PPF) cells, which met the first criterion.
68 These neurons were present in ~5 distinct clusters, each containing ~1-3 PPF cells, within a
69 relatively small brain region (see Fig. 1a). Cells in one such cluster, PPF1 (Fig. 1b, #6) exhibited
70 a median $\tau \sim 83$ s (ED Fig. 1g, h). Cells in three other clusters including PPF2 (Fig. 1b, #3), showed
71 a median $\tau > \sim 75$, but failed to meet the second and third criteria. Another cluster in addition to
72 PPF1 met all 3 criteria, but was not genetically accessible.

73 To gain specific genetic access to PPF1 neurons, we first examined the anatomy of these cells
74 by combining P1 stimulation-evoked GCaMP imaging with photo-activatable GFP (PA-GFP)
75 labeling of responding cells²³. We generated a nuclear-localized GCaMP (NLS-GCaMP6s) to
76 prevent cytoplasmic GCaMP signal from obscuring PA-GFP fluorescence (Fig. 1c₁). NLS-
77 GCaMP6s also detected persistent responses to P1 stimulation in PPF1 cells (Fig. 1c₂). We then
78 focused a 720 nm two-photon laser on the identified PPF1 cells, and revealed their projection
79 pattern via diffusion of activated PA-GFP²³ (Fig. 1c₃). By comparing the morphology of PPF1
80 neurons with Fru-MARCM^{24,25} and Gal4 line image databases²⁶, we identified two Gal4 drivers,
81 R41A01 and R21D06, which labeled morphologically similar neurons (Fig. 1c₄, d; ED Fig. 2a-d).
82 To verify that R41A01 and R21D06 indeed label PPF1 neurons, we performed functional imaging
83 in R41A01>GCaMP6s or R21D06>GCaMP6s flies, and confirmed persistent responses to P1
84 activation in PPF1 somata (Fig. 1e and ED Fig. 2c); whether such persistent responses are present
85 in all neurites is difficult to ascertain. Interestingly, these neurons exhibited stepwise integration
86 of P1 input (Fig. 1e); however repeated P1 stimulation trials (as done in volume imaging, 30 trials,
87 Fig. 1b) sensitized PPF1 neurons (ED Fig. 3).

88 Gal4 line R41A01 labels a cell cluster called pCd, previously reported to play an important
89 role in female sexual receptivity²⁷. Analysis of marker expression indicated that pCd cells are

90 cholinergic neurons that express both Fru and Dsx (ED Fig. 2f-i), two sex-determination factors
91 that label neurons involved in male courtship and aggression^{3,8,28-31}. pCd neurons project densely
92 to the superior-medial protocerebrum (SMP), while extending an additional long fiber bundle
93 ventrally to innervate the dorsal region of the subesophageal zone (SEZ; Fig. 1d). Double labeling
94 of pCd neurons with somatodendritic (Denmark-RFP³²) and pre-synaptic (Syt-GFP³³) markers
95 revealed that their SMP projections are mostly dendritic, while their pre-synaptic terminals are
96 located in the SMP and the SEZ (ED Fig. 4d-f). Registration of P1 pre-synaptic labeling with pCd
97 somatodendritic labeling in a common brain template failed to reveal clear overlap (ED Fig. 4g-i),
98 and application of the GFP Reconstitution Across Synaptic Partner (GRASP³⁴) technique failed to
99 detect close proximity between P1 and pCd neurons (ED Fig. 4j-r), suggesting that functional
100 connectivity between these cells is unlikely to be monosynaptic.

101 **pCd neuronal activity is required for P1-induced persistent social behaviors**

102 To test whether P1-evoked persistent social behaviors require pCd activity, we silenced the
103 latter using R41A01-LexA>LexAop-Kir2.1 while activating P1^a-split GAL4 neurons using UAS-
104 Chrimson. In solitary males (Fig. 2a), silencing pCd neurons dramatically reduced persistent wing
105 extension evoked by Chrimson activation of P1 cells (Fig. 2b vs. 2c, green shading; 2d).
106 Importantly, time-locked wing-extension during photostimulation was unaffected (Fig. 2b-d, gray
107 shading). Persistent aggression evoked by P1 activation in pairs of males^{9,35} (Fig. 2e, f) was also
108 strongly reduced by silencing pCd neurons (Fig. 2g, h, blue shading), while wing-extension during
109 photostimulation was unaffected. This result was confirmed using a more specific
110 R41A01∩R21D06 intersectional split-GAL4 driver (ED Fig. 2d) to silence pCd neurons, and
111 R15A01-LexA to activate P1 cells (ED Fig. 5). Thus pCd activity is required for enduring, but not
112 for time-locked, behavioral responses to P1 activation.

113 **pCd neurons amplify and prolong, but do not trigger, social behaviors**

114 We next investigated the effect on behavior of optogenetically stimulating pCd neurons.
115 Interestingly, optogenetic activation of pCd neurons in solitary flies had no visible effect, in
116 contrast to optogenetic activation of P1 neurons^{4,9,15} (Fig. 3a, b). Persistent internal states can
117 change an animal's behavioral response to sensory cues. We reasoned that if pCd neurons promote
118 such a persistent internal state, then their optogenetic activation, while insufficient to evoke
119 behavior on its own, might nevertheless suffice to modify the behavioral response of the flies to
120 an external social stimulus. To test this, we examined the effect of pCd stimulation on the
121 behavioral response of males to female cues (Fig. 3d). Activation of pCd neurons in the presence
122 of a dead female dramatically elevated courtship behavior during photostimulation, and this effect
123 persisted for several minutes after stimulus offset (Fig. 3b vs. 3e, pCd>Chrimson; Fig. 3c, f, pCd).

124 Activation of pCd neurons in pairs of non-aggressive group-housed male flies did not promote
125 aggression, unlike P1 activation⁹ (Fig. 3g-i). But in the presence of a dead female, which produced
126 increased baseline aggression in male flies³⁶, activation of pCd neurons significantly enhanced fly
127 aggressiveness after photostimulation, an effect not observed in photostimulated controls (Fig. 3j-
128 l). Thus, unlike P1 activation, which can substitute for the effect of dead females to trigger
129 courtship or aggression, pCd activation alone cannot do so (Fig. 3b-c, h-i). However pCd neuron
130 activation can enhance and extend the effect of a dead female to promote these social behaviors.

131 **pCd neurons are required for sustained courtship and aggressive drive**

132 Given that pCd neuronal activity is required for optogenetic P1 activation-evoked social
133 behavior (Fig. 2), we next investigated its requirement during natural social behavior. Silencing
134 pCd neurons significantly increased the latency to copulation (ED Fig. 6a, b). To examine the

135 effect of silencing on courtship *per se*, without rapid progression to copulation, we tested males in
136 the presence of a freeze-killed virgin female, which induced robust unilateral wing-extensions
137 (UWEs; courtship song³⁷). In controls (BDP-GAL4> Kir2.1 or GFP), the fraction of flies
138 exhibiting UWEs was relatively constant across the 15 min assay (Fig. 4a, BDP, gray and red
139 lines). However in pCd>Kir2.1 flies, UWEs declined significantly during that interval, in
140 comparison to pCd>GFP controls (Fig. 4a, pCd, red line, green vs blue shading).

141 We next performed parallel experiments for aggression. Single-housed (SH) male flies will
142 fight on food in the absence of females^{36,38}, and the intensity of fighting escalates over time (Fig.
143 4b, BDP). However in SH pCd>Kir2.1 flies, aggression did not escalate over time, although initial
144 levels of lunging were similar to controls (Fig. 4b, pCd, blue line, green vs. blue shading). These
145 data demonstrate a requirement for pCd neurons in escalated aggression, independent of any
146 influence from females. Importantly, in both assays, silencing pCd neurons did not impair
147 initiation of social behavior, consistent with the inability of pCd optogenetic stimulation to trigger
148 these behaviors (Fig. 3b, g); rather it influenced their amplitude and kinetics.

149 The effect of pCd silencing on courtship vs. aggression was subtly different: in the former case,
150 silencing pCd neurons caused UWEs to steadily decline over time, whereas during aggression,
151 natural escalation failed to occur (Fig. 4a vs. 4b, pCd, red vs. blue lines). To investigate whether a
152 common mechanism could explain both phenotypes, we asked whether both data could be jointly
153 fit by a “leaky integrator” model³⁹. Such models formalize classical “hydraulic” theories of
154 behavioral drive⁴⁰, in which the instantaneous level of activity in a neural integrator circuit
155 determines either the rate or type of an animal’s behavior; here, we sought to fit the time-evolving
156 rate of UWEs, or of lunging (Fig. 4c). Our leaky integrator model assumed that flies received
157 sensory input from conspecifics with a rate constant R , and that the activity of the neural circuit

158 integrating conspecific sensory cues decayed from its initial condition to steady-state with a “leak”
159 rate constant T (min^{-1}).

160 The behavioral data in each assay were well fit by models in which the only free parameter
161 allowed to vary by genotype was T (Fig. 4c-e). For UWEs, in control flies the relatively flat line
162 reflects the fact that the initial rate of behavior is high, and already close to the steady-state where
163 “fill” and “leak” rates are equal (Fig. 4f, left). In contrast, the faster decline of UWEs in
164 $pCd>Kir2.1$ flies (Fig. 4c) was best fit by an increase in T (Fig. 4e, red bars). During aggression,
165 control flies exhibit escalation (Fig. 4d, $BDP>Kir2.1$) because the initial rate of aggression is low,
166 and the sensory input rate constant R is greater than T for this behavior (Fig. 4g, left). Increasing
167 T in $pCd>Kir2.1$ flies therefore converts aggression to a relatively flat line (Fig. 4d; 4g, right).
168 Thus, the superficially different courtship vs. aggression phenotypes caused by silencing pCd
169 neurons can be explained by a common mechanism, whereby inhibition of pCd neurons increases
170 the leak rate constant of a neural integrator, which may control a state of social arousal or drive^{20,41}.

171 **pCd neurons display neural integrator properties**

172 We next investigated whether pCd neurons display integrator properties at the level of their
173 physiology. The observation that they exhibit stepwise summation of P1 input (Fig. 1e, ED Fig.
174 3a) is consistent with this idea. Surprisingly, repeated direct stimulation of PPF1 neurons did not
175 exhibit such summation, and evoked faster-decaying responses (median $\tau \sim 13.4$ s) than evoked by
176 indirect P1 activation (median $\tau \sim 83$ s), indicating that persistent activity cannot be triggered cell
177 autonomously (Fig. 5a). However, pCd function might be necessary, although not sufficient, for
178 persistent activity (Fig. 5b, right). If so, then persistent pCd activity should not recover from
179 transient inhibition performed during the decay phase following P1 stimulation^{42,43}. Alternatively,

180 if pCd cells simply “inherit” persistence passively from an upstream input (Fig. 5b, left), their
181 persistent P1 response should recover following transient inhibition. We therefore stimulated P1
182 neurons (5 s) whilst imaging from pCd cells, and after a short delay (25 s) briefly (~10 s) inhibited
183 pCd activity using the green light-sensitive inhibitory opsin GtACR1⁴⁴ and 2-photon spiral
184 scanning⁴⁵ at 1070 nm to restrict inhibition to pCd cells (Fig. 5e, f and Methods).

185 Actuation of GtACR1 in pCd neurons following P1 stimulation caused a rapid, ~68% decrease
186 in $\Delta F/F$ signal, which did not recover to control levels following the offset of inhibition, but rather
187 remained flat (Fig. 5g₂, blue shaded area, solid vs. dashed line and Fig. 5h, pCd, green bar). This
188 effect is not due to irreversible damage to pCd neurons by photo-inhibition, since reactivation of
189 P1 neurons following transient pCd inhibition reliably re-evoked pCd persistent activity, and
190 multiple cycles of P1 stimulation with or without GtACR1 actuation could be performed with
191 consistent results (ED Fig. 7a, b, pCd). Furthermore, 2-photon spiral scanning at 1070 nm of pCd
192 neurons lacking GtACR1 had no effect (Fig. 5g₃), confirming that the decrease in GCaMP signal
193 is due to inhibition of activity by GtACR1 and not to 2-photon irradiation. As the experiment was
194 originally performed using Fru-LexA to label pCd cells, we confirmed the result using a pCd-
195 specific driver (ED Fig. 8, blue shading).

196 As an additional control, we also performed the same manipulation on PPF2 neurons, another
197 FruM⁺ population located near pCd (Fig. 5c), which also showed persistent responses to P1
198 activation (Fig. 1b₃; Fig. 5d, PPF2). In this case, following GtACR inhibition PPF2 activity
199 quickly recovered to the level observed at the equivalent time-point in controls without 1070 nm
200 photo-inhibition (Fig. 5g₅, 5h, PPF2 and ED Fig. 7b, PPF2). Thus, PPF2 activity is not required
201 continuously to maintain a persistent response to P1 activation. In contrast, persistence in pCd
202 neurons requires their continuous activity. However the fact that persistent activity cannot be

203 evoked by direct stimulation of pCd neurons alone suggests that persistence likely requires co-
204 activation of a network comprised of multiple neurons.

205 **pCd neurons are required for an effect of females to persistently enhance male**
206 **aggressiveness, and are activated by an aggression-promoting pheromone, cVA**

207 The foregoing data indicated that pCd neurons are required to maintain a P1 activation-
208 triggered persistent internal state, which prolongs wing extension in solitary males and promotes
209 aggression when male flies encounter another male. We next asked whether pCd neurons are
210 similarly required for a persistent internal state triggered by naturalistic cues. Since P1 neurons are
211 activated by female cues (reviewed in ref. ¹⁴), we examined the influence of transient female
212 exposure on male aggressive behavior. Previous studies have demonstrated that females can
213 enhance inter-male aggression (ref^{36,46} and see Fig. 3h vs. k), but whether this effect can persist
214 following the removal of females was not clear. To investigate this, we pre-incubated individual
215 male flies for 5 min with or without a live female, and then gently transferred them into an agarose-
216 covered arena to measure their aggression (Fig. 6a). Male flies pre-incubated with a female showed
217 significantly higher levels of lunging than controls (Fig. 6b), indicating a persistent influence of
218 female exposure to enhance aggressiveness.

219 We next asked whether this persistent influence requires continuous pCd activity. To do this,
220 male flies expressing GtACR1 in pCd neurons were pre-incubated with females, and briefly
221 photostimulated with green light during the aggression test (Fig. 6c). Transient inhibition of pCd
222 neurons abrogated the effect of female pre-exposure to enhance aggression (Fig. 6d), mirroring the
223 effect of such transient inhibition to disrupt persistent physiological activity in these cells (Fig.
224 5g₂). Thus, continuous pCd neuron activity is required to maintain a persistent behavioral state

225 change induced by female presentation. Importantly, this effect was not observed when P1 neurons
226 were transiently silenced using GtACR, although such silencing of P1 cells did transiently disrupt
227 male courtship towards females (ED Fig. 9), as previously reported¹⁷.

228 The foregoing experiments indicated that when males are removed from the presence of
229 females and confronted with another male, their behavior switches from courtship to aggression.
230 To investigate whether pCd neurons themselves might also play a role in the detection of male
231 cues that trigger this behavioral switch, we investigated whether they can respond to 11-cis
232 Vaccenyl Acetate (cVA), a male-specific pheromone that has been shown to promote aggression⁴⁷
233 (Fig. 6e). Notably, cVA has already been shown to activate pCd cells in females²⁷, where the
234 pheromone promotes sexual receptivity. Although other pheromones have been shown to promote
235 male aggression in *Drosophila*, such as 7-tricosene⁴⁸, the non-volatility of that compound made it
236 difficult to deliver in a controlled manner to walking flies in our imaging preparation (Fig. 6f)
237 without physically disturbing them.

238 To do this, we imaged pCd activity using GCaMP6s in flies exposed to the following stimuli
239 at 5 minute intervals: 10 s of P1 activation; cVA vapour presentation; or P1 stimulation (10 s)
240 followed 30 s later by cVA (Fig. 6g₁₋₃). Among pCd neurons persistently activated by P1
241 stimulation (Fig. 6g₁), only half responded to cVA alone (defined as $>2\sigma$ above baseline; Fig. 6g₂).
242 However, delivery of cVA 30 s after P1 stimulation (i.e., during the persistent phase of the
243 response) yielded cVA responses ($>2\sigma$ above post-P1 activity) in 90% of the pCd cells (Fig. 6g₃).
244 Moreover, peak cVA responses were significantly greater following P1 activation, than in flies
245 exposed to the pheromone on its own (median increase 1.8-fold; Fig. 6h, i). Thus, individual pCd
246 neurons that are activated by P1 stimulation in males can also respond to cVA (Fig. 6e), and this
247 response is enhanced during the persistent phase of the P1 response.

248 **DISCUSSION**

249 Optogenetic activation of P1 neurons evokes both courtship song, in a reflexive manner^{15,16},
250 and a persistent internal state of arousal or drive²⁰ that promotes aggression in the presence of a
251 conspecific male^{9,35}. Here we have identified a population of indirect persistent P1 follower cells,
252 called pCd neurons²⁷, whose activity is necessary for P1-triggered persistent aggression. pCd
253 neurons are also necessary for persistent UWEs triggered by P1 activation, on a time scale
254 outlasting P1 activity (as measured in separate imaging experiments). An earlier study¹⁷ reported
255 that P1 activity is continuously required during male courtship following initial female contact,
256 but did not distinguish whether this requirement reflected continuous stimulation of P1 cells by
257 non-contact-dependent female-derived cues (e.g., motion cues^{11,14}), or a true fly-intrinsic persistent
258 response. In contrast, the use of transient optogenetic stimulation here clearly demonstrates
259 persistent fly-intrinsic responses. Nevertheless we cannot exclude that persistent P1 activity may
260 occur during natural courtship bouts¹⁷. Importantly, however, we show that pCd but not P1 neurons
261 are required for a persistent increase in aggressive state induced by transient female pre-exposure
262 (Fig. 6d). Together, these data suggest that pCd neurons participate in a network that may encode
263 a persistent memory of a female, which can be combined with the detection of an opponent male
264 at a later time to elicit aggression^{9,20}. The observation that P1 neuron activation enhances pCd
265 responses to cVA, an aggression-promoting pheromone⁴⁷, is consistent with this idea.

266 Our physiological data suggest that pCd neurons are part of a circuit that temporally integrates
267 P1 input to yield a slow response that decays over minutes (Fig. 1e). The fact that transiently
268 silencing pCd neurons using GtACR irreversibly interrupts this slow response argues that it indeed
269 reflects persistent pCd activity, and not simply persistence of GCaMP6s fluorescence. It is likely
270 that this integrator circuit comprises additional neurons, including non-Fru-expressing neurons.

271 Evidently, P1 neurons activate this circuit in parallel with a “command” network, including pIP10
272 descending interneurons^{7,49}, that triggers rapid-onset courtship behavior. These results illustrate
273 how acute and enduring responses to sensory cues may be segregated into parallel neural pathways,
274 allowing behavioral control on different time scales, with different degrees of flexibility (Fig. 6j).
275 The incorporation of parallel neural pathways that allow behavioral responses to stimuli to be
276 processed on multiple timescales may represent an important step in the evolution of behavior,
277 from simple stimulus-response reflexes to more integrative, malleable responses^{41,50,51}.

278 Our data raise several new and interesting questions for future investigation. First, what cells
279 provide direct synaptic inputs to pCd neurons, and what is the connectional relationship of these
280 cells to P1 neurons? Second, the fact that pCd activity is necessary but not sufficient to trigger
281 persistence suggests that other cells likely contribute to the integrator circuit; what are these cells
282 (Fig. 6j, Y, Z)? Finally, how is persistence encoded, and what is the role of pCd neurons in
283 determining its duration? The data presented here provide insight into the complex networks that
284 underlie behavioral temporal dynamics^{17,52} in *Drosophila*, and offer a useful point-of-entry to
285 this fascinating problem.

286 **Acknowledgements**

287 We thank H. Inagaki for comments on the manuscript, B. Pfeiffer and G. M. Rubin for fly
288 strains, A. M. Wong for help with initial development of all-optical stimulation and imaging, A.
289 Sanchez for maintaining fly stocks, C. Chiu for lab management and G. Mancuso for
290 administrative assistance. This work was supported in part by NIH grant R01 DA031389. D.J.A.
291 is an Investigator of the Howard Hughes Medical Institute. The authors declare no conflicts-of-
292 interest.

293 **Author Contributions**

294 D.A. and Y.J. conceived the project, designed experiments and co-wrote the manuscript; Y.J.
295 performed all experiments, collected and analyzed data and prepared figures; A.K. performed
296 mathematical modeling studies; H.C. generated R41A01-AD, R41A01-DBD, and nuclear-
297 localized GCaMP6s constructs and flies; M.F. and A.C.-C. provided unpublished LexAop-GtACR
298 flies.

299 **Data Availability**

300 Datasets generated during the current study are available from the corresponding author on
301 reasonable request.

302 **References**

- 303 1 Tinbergen, N. *The study of instinct*. (Clarendon Press, 1951).
- 304 2 Bargmann, C. I. Beyond the connectome: How neuromodulators shape neural circuits.
305 *Bioessays* **34**, 458-465, (2012).
- 306 3 Yamamoto, D. & Koganezawa, M. Genes and circuits of courtship behaviour in *Drosophila*
307 males. *Nature Rev. Neurosci.* **14**, 681-692, (2013).
- 308 4 Clowney, E. J., Iguchi, S., Bussell, J. J., Scheer, E. & Ruta, V. Multimodal Chemosensory
309 Circuits Controlling Male Courtship in *Drosophila*. *Neuron*, (2015).
- 310 5 Kallman, B. R., Kim, H. & Scott, K. Excitation and inhibition onto central courtship
311 neurons biases *Drosophila* mate choice. *eLife* **4**, 2027, (2015).
- 312 6 Kohatsu, S., Koganezawa, M. & Yamamoto, D. Female contact activates male-specific
313 interneurons that trigger stereotypic courtship behavior in *Drosophila*. *Neuron* **69**, 498-508,
314 (2011).

- 315 7 von Philipsborn, A. C. *et al.* Neuronal control of *Drosophila* courtship song. *Neuron* **69**,
316 509-522, (2011).
- 317 8 Pan, Y., Robinett, C. C. & Baker, B. S. Turning males on: activation of male courtship
318 behavior in *Drosophila melanogaster*. *PloS one* **6**, e21144, (2011).
- 319 9 Hoopfer, E. D., Jung, Y., Inagaki, H. K., Rubin, G. M. & Anderson, D. J. P1 interneurons
320 promote a persistent internal state that enhances inter-male aggression in *Drosophila*. *eLife*
321 **4**, (2015).
- 322 10 Zhang, S. X., Rogulja, D. & Crickmore, M. A. Dopaminergic Circuitry Underlying Mating
323 Drive. *Neuron* **91**, 168-181, (2016).
- 324 11 Kohatsu, S. & Yamamoto, D. Visually induced initiation of *Drosophila* innate courtship-
325 like following pursuit is mediated by central excitatory state. *Nature Communications* **6**,
326 (2015).
- 327 12 Zhang, W., Guo, C., Chen, D., Peng, Q. & Pan, Y. Hierarchical Control of *Drosophila* Sleep,
328 Courtship, and Feeding Behaviors by Male-Specific P1 Neurons. *Neuroscience bulletin*,
329 (2018).
- 330 13 Chen, D. *et al.* Genetic and neuronal mechanisms governing the sex-specific interaction
331 between sleep and sexual behaviors in *Drosophila*. *Nat Commun* **8**, 154, (2017).
- 332 14 Auer, T. O. & Benton, R. Sexual circuitry in *Drosophila*. *Curr Opin Neurobiol* **38**, 18-26,
333 (2016).
- 334 15 Inagaki, H. K. *et al.* Optogenetic control of *Drosophila* using a red-shifted
335 channelrhodopsin reveals experience-dependent influences on courtship. *Nat Methods*, -,
336 (2014).
- 337 16 Bath, D. E. *et al.* in *Nat Methods* Vol. 11 756-762 (2014).

- 338 17 Zhang, S. X., Miner, L. E., Boutros, C. L., Rogulja, D. & Crickmore, M. A. Motivation,
339 Perception, and Chance Converge to Make a Binary Decision. *Neuron* **99**, 376-388 e376,
340 (2018).
- 341 18 Hoopfer, E. D. Neural control of aggression in *Drosophila*. *Curr Opin Neurobiol* **38**, 109-
342 118, (2016).
- 343 19 Klapoetke, N. C. *et al.* in *Nat Methods* Vol. 11 338-346 (Nature Publishing Group, 2014).
- 344 20 Anderson, D. J. Circuit modules linking internal states and social behaviour in flies and
345 mice. *Nature reviews. Neuroscience* **17**, 692-704, (2016).
- 346 21 Chen, T. W. *et al.* Ultrasensitive fluorescent proteins for imaging neuronal activity. *Nature*
347 **499**, 295-300, (2013).
- 348 22 Mellert, D. J., Knapp, J. M., Manoli, D. S., Meissner, G. W. & Baker, B. S. Midline crossing
349 by gustatory receptor neuron axons is regulated by *fruitless*, *doublesex* and the Roundabout
350 receptors. *Development* **137**, 323-332, (2010).
- 351 23 Datta, S. R. *et al.* The *Drosophila* pheromone cVA activates a sexually dimorphic neural
352 circuit. *Nature* **452**, 473-477, (2008).
- 353 24 Cachero, S., Ostrovsky, A. D., Yu, J. Y., Dickson, B. J. & Jefferis, G. S. X. E. Sexual
354 dimorphism in the fly brain. *Curr Biol* **20**, 1589-1601, (2010).
- 355 25 Chiang, A. S. *et al.* Three-dimensional reconstruction of brain-wide wiring networks in
356 *Drosophila* at single-cell resolution. *Curr Biol* **21**, 1-11, (2011).
- 357 26 Jenett, A. *et al.* A GAL4-driver line resource for *Drosophila* neurobiology. *Cell reports* **2**,
358 991-1001, (2012).
- 359 27 Zhou, C., Pan, Y., Robinett, C. C., Meissner, G. W. & Baker, B. S. Central brain neurons
360 expressing *doublesex* regulate female receptivity in *Drosophila*. *Neuron* **83**, 149-163,

- 361 (2014).
- 362 28 Stockinger, P., Kvitsiani, D., Rotkopf, S., Tirián, L. & Dickson, B. J. Neural circuitry that
363 governs *Drosophila* male courtship behavior. *Cell* **121**, 795-807, (2005).
- 364 29 Manoli, D. S. *et al.* Male-specific fruitless specifies the neural substrates of *Drosophila*
365 courtship behaviour. *Nature* **436**, 395-400, (2005).
- 366 30 Kimura, K.-I., Hachiya, T., Koganezawa, M., Tazawa, T. & Yamamoto, D. in *Neuron* Vol.
367 59 759-769 (2008).
- 368 31 Rideout, E. J., Billeter, J.-C. & Goodwin, S. F. The sex-determination genes fruitless and
369 doublesex specify a neural substrate required for courtship song. *Current biology : CB* **17**,
370 1473-1478, (2007).
- 371 32 Nicolai, L. J. *et al.* Genetically encoded dendritic marker sheds light on neuronal
372 connectivity in *Drosophila*. *Proc Natl Acad Sci U S A* **107**, 20553-20558, (2010).
- 373 33 Zhang, Y. Q., Rodesch, C. K. & Broadie, K. Living synaptic vesicle marker:
374 synaptotagmin-GFP. *Genesis* **34**, 142-145, (2002).
- 375 34 Feinberg, E. H. *et al.* GFP Reconstitution Across Synaptic Partners (GRASP) defines cell
376 contacts and synapses in living nervous systems. *Neuron* **57**, 353-363, (2008).
- 377 35 Watanabe, K. *et al.* A Circuit Node that Integrates Convergent Input from Neuromodulatory
378 and Social Behavior-Promoting Neurons to Control Aggression in *Drosophila*. *Neuron* **95**,
379 1112-1128 e1117, (2017).
- 380 36 Lim, R. S., Eyjolfsdottir, E., Shin, E., Perona, P. & Anderson, D. J. How food controls
381 aggression in *Drosophila*. *PloS one* **9**, e105626, (2014).
- 382 37 Tauber, E. & Eberl, D. F. in *Behav Processes* Vol. 64 197-210 (2003).
- 383 38 Wang, L., Dankert, H., Perona, P. & Anderson, D. J. A common genetic target for

- 384 environmental and heritable influences on aggressiveness in *Drosophila*. *Proc. Natl. Acad.*
385 *Sci. USA* **105**, 5657-5663, (2008).
- 386 39 Chaudhuri, R. & Fiete, I. Computational principles of memory. *Nature neuroscience* **19**,
387 394-403, (2016).
- 388 40 Lorenz, K. & Leyhausen, P. *Motivation of human and animal behavior; an ethological*
389 *view*. Vol. xix (Van Nostrand-Reinhold, 1973).
- 390 41 Anderson, David J. & Adolphs, R. A Framework for Studying Emotions across Species.
391 *Cell* **157**, 187-200, (2014).
- 392 42 Guo, Z. V. *et al.* Maintenance of persistent activity in a frontal thalamocortical loop. *Nature*
393 **545**, 181-186, (2017).
- 394 43 Inagaki, H. K., Fontolan, L., Romani, S. & Svoboda, K. Discrete attractor dynamics
395 underlies persistent activity in the frontal cortex. *Nature* **566**, 212-217, (2019).
- 396 44 Mohammad, F. *et al.* Optogenetic inhibition of behavior with anion channelrhodopsins.
397 *Nat Methods*, (2017).
- 398 45 Rickgauer, J. P. & Tank, D. W. Two-photon excitation of channelrhodopsin-2 at saturation.
399 *Proceedings of the National Academy of Sciences of the United States of America* **106**,
400 15025-15030, (2009).
- 401 46 Lim, R. S. *PhD Thesis*, California Institute of Technology, (2014).
- 402 47 Wang, L. & Anderson, D. J. Identification of an aggression-promoting pheromone and its
403 receptor neurons in *Drosophila*. *Nature* **463**, 227-231, (2010).
- 404 48 Wang, L. *et al.* Hierarchical chemosensory regulation of male-male social interactions in
405 *Drosophila*. *Nature neuroscience* **14**, 757-762, (2011).
- 406 49 Ding, Y. *et al.* Neural Evolution of Context-Dependent Fly Song. *Curr Biol* **29**, 1089-1099

407 e1087, (2019).

408 50 Gibson, William T. *et al.* Behavioral Responses to a Repetitive Visual Threat Stimulus
409 Express a Persistent State of Defensive Arousal in *Drosophila*. *Current Biology* **25**, 1401-
410 1415, (2015).

411 51 Bach, D. R. & Dayan, P. in *Nature reviews. Neuroscience* Vol. 18 311-319 (2017).

412 52 Crickmore, M. A. & Vosshall, L. B. Opposing dopaminergic and GABAergic neurons
413 control the duration and persistence of copulation in *Drosophila*. *Cell* **155**, 881-893, (2013).

414 **METHODS**

415 **Rearing conditions.** Flies were reared under standard conditions at 25°C and 55% humidity, on a
416 12 h light/12 h dark cycle. 2-5 days old virgin females were used to cross with different male stocks.
417 The density of experimental flies (-5 pupae/cm²) was controlled by limiting the number of parents;
418 crosses with too high or too low density of progeny were discarded. Male flies were collected 0-2
419 days after eclosion and reared either individually (single-housed) or at 18 flies (group-housed) per
420 vial for 5-6 days before the behavioral assays. Newly eclosed males were excluded from collection.
421 For optogenetic experiments, eclosed males were reared in the dark with food containing 0.4 mM
422 all-*trans*-retinal (Sigma-Aldrich, St. Louis, MO). For two-color optogenetic experiments, flies
423 were reared in the dark from larval stage. Virgin females provided during behavioral tests were
424 reared at high density (30 flies per vial) for 2-3 days. Flies carrying Gal4 and UAS-opsin
425 transgenes were maintained in the dark to prevent uncontrolled activation of the opsins.

426 **Fly strains.** The following lines were generated in this study. *R41A01-LexA* (*vk00027* and *attp2*),
427 *R41A01-AD* (*attp40*), and *R41A01-DBD* (*attp2*) were constructed based on the methods described
428 in ref⁵³. *R41A01* enhancer fragment was amplified from genomic DNA based on sequences in
429 (ref⁵⁴). The primers used for amplification were designed based on recommendations in the *Janelia*

430 FlyLight project and Bloomington Drosophila Stock Center
431 (https://bdsc.indiana.edu/stocks/gal4/gal4_janelia.html). For making *LexAop2-NLS-GCaMP6s*
432 (*su(Hw)attp5*), two nuclear localization signal (NLS) peptides, one from SV40 and the other from
433 the *Drosophila* gene *scalloped*, were used. SV40-NLS (ccaagaagaaaaggaagta) was fused to the
434 5' end, and the scalloped-NLS
435 (agaaccaggaagcaagtcagttcgcatccaagtgtgctgctgccgtaaactccgcgagatc) was fused to the 3' end of
436 the codon-optimized GCaMP6s. A DNA fragment containing *syn21-SV40-NLS-GCaMP6s-*
437 *scalloped-NLS* was ligated into pJFRC19-13LexAop2-IVS-myr::GFP-sv40 (Addgene plasmid #
438 26224) via XhoI and XbaI restriction enzyme sites. The sv40 terminator in the pJFRC19 was
439 replaced with p10 terminator via XbaI and FseI sites. To generate LexAop-GtACR1 flies, the
440 GtACR1 *Drosophila*-codon-optimized sequence⁴⁴ was subcloned into pJFRC19-13LexAop2-IVS-
441 myr::GFP-sv40 (Addgene plasmid # 26224) plasmid. The GtACR1::eYFP fragment was swapped
442 with the myr::GFP fragment using XhoI and XbaI. *15A01-LexA (attp2)*, *BDP-AD (attp40)* and
443 *BDP-DBD (attp2)*, *10xUAS-NLS-tdTomato (VK00040)*, *13xLexAop2-NLS-GFP (VK00040)*,
444 *10xUAS-Chrimson::tdTomato (su(Hw)attp1 and attp18)*, *20XUAS-Chrimson::tdTomato*
445 (*su(Hw)attp5*), *13xLexAop2-myr::tdTomato (attp18)*, *13xLexAop2-OpGCaMP6s (su(Hw)attp8)*,
446 *20xUAS-OpGCaMP6s (su(Hw)attp5)*, *13xLexAop2-mPA-GFP (su(Hw)attp8)*, *13xLexAop2-*
447 *Kir2.1::eGFP (VK00027)*, *10xUAS-Kir2.1::eGFP (attp2)*, *10xUAS-GFP (attp2)*, *R21D06-LexA*
448 (*attp2*) were from G. Rubin; *dsx-DBD* was from S. Goodwin⁵⁵; *Fru-LexA* was from B. Baker²²;
449 *Orco-LexA* was from T. Lee⁵⁶; *UAS-CD4::spGFP1-10* and *LexAop-CD4::spGFP11* were from K.
450 Scott⁵⁷; *20XUAS-GtACR1::eYFP (attp2)* was from A. Claridge-Chang; Wild-type Canton S was
451 from M. Heisenberg⁵⁸.

452 The following lines were obtained from the Bloomington Stock Center: *BDP-LexA (attp40)*

453 (77691), *71G01-Gal4 (attp2)* (39599), *71G01-DBD (attp2)* (69507), *15A01-Gal4 (attp2)* (48670),
454 *15A01-AD (attp40)* (68837), *R41A01-Gal4 (attp2)* (39425), *R41A01-LexA (attp40)* (54787),
455 *R21D06-DBD (attp2)* (69873), *ChAT-DBD* (60318), *VGlut-DBD* (60313), *Gad1-p65AD* (60322),
456 *UAS-Denmark*; *UAS-Syt-eGFP* (33064), *GH146-Gal4* (30026), *13XLexAop2-*
457 *CsChrimson::mVenus (attp40)* (55138), *10XUAS-myr::GFP (su(Hw)attp8)* (32196), *10XUAS-*
458 *myr::GFP (attp2)* (32197), *UAS-Kir2.1::eGFP* (6595).

459 **Two-photon GCaMP imaging.** Calcium imaging was performed using a custom-modified Ultima
460 two-photon laser scanning microscope (Bruker). The primary beam path was equipped with
461 galvanometers driving a Chameleon Ultra II Ti:Sapphire laser (Coherent) and used for GCaMP
462 imaging (920 nm). The secondary beam path was equipped with separate set of galvanometers
463 driving a Fidelity-2 Fiber Oscillator laser (Coherent) for GtACR1 actuation (1070 nm). The two
464 lasers were combined using 1030 nm short-pass filter (Bruker). GCaMP emission was detected
465 with photomultiplier-tube (Hamamatsu). Images were acquired with an Olympus 40x, 0.8
466 numerical aperture objective (LUMPLFLN) equipped with high-speed piezo-z (Bruker). All
467 images acquisition was performed using PrairieView Software (Version 5.3). For fast volume
468 imaging (Fig. 1a, b and ED Fig. 1), three 4- μ m optical sections were collected at 180 X 180 pixel
469 resolution with a frame rate \sim 0.83 Hz. All of the other images were acquired at 256 X 256 pixel
470 resolution with a frame rate 1 Hz. Saline (108 mM NaCl, 5 mM KCl, 4 mM NaHCO₃, 1 mM
471 NaH₂PO₄, 5 mM trehalose, 10 mM sucrose, 5 mM HEPES, 0.5 mM CaCl₂, 2 mM MgCl₂, pH=7.5)
472 was used to bathe the brain during functional imaging. Saline containing 90 mM KCl was added
473 for high-resolution z stack after functional imaging to verify cell identity in ED Figure 1.

474 To prepare flies in vivo imaging, 6-8 days old flies were anesthetized on a cold plate and mounted
475 on a thin plastic plate with wax. The wings, all legs, antenna, and arista were kept intact, wax-free,

476 and free to move. Saline was added on the top side of the plate to submerge the fly head. A hole in
477 the posterior-dorsal side of the head was opened using sharp forceps. Animals were then placed
478 beneath the objective, and a plastic ball supported with air was positioned under the fly. The
479 conditions inside of the imaging setup were maintained similar to the rearing conditions (25°C and
480 55% humidity). The flies were habituated for 30 min, and their behaviors were observed from the
481 side using Point Grey Flea3 camera mounted with 0.5x-at-94 mm Infinistix lens fitted with a
482 bandpass IR filter (830 nm, Edmund Optics) to block the two photon imaging laser and optogenetic
483 stimulation lights. Animals that exhibited no movement, strenuous movement, and prolonged
484 abdomen bending during and after habituation were discarded.

485 Chrimson activation during calcium imaging was performed as described in ref¹⁵. A deep red (660
486 nm) fiber-coupled LED (Thorlab) with band-pass filter (660 nm, Edmund Optics) was used for
487 light source to activate Chrimson. A 200 μm core multimode optic fiber placed 200 μm away from
488 the brain was used to deliver 10 Hz, 10 ms pulse-width light. The light intensity at the tip of optic
489 fiber was set to be 39.2 μW . For two photon GtACR1 actuation, 1070 nm laser (Fidelity-2,
490 Coherent) was delivered by galvanometers to a circular area with diameter $\approx 15 \mu\text{m}$ containing 1-
491 3 cell bodies in focus for -10 s by spiral scanning (10 $\mu\text{m}/\text{pixel}$, 45.24 ms/repeat, 220 repeats).
492 Galvanometers were re-calibrated weekly using a slide glass coated with thin layer of fluorescent
493 dye. Field of view was adjusted in order to keep the spiral scanning area near the center of the
494 imaging field. cVA was presented by directing a continuous airstream (80 mL/min) through a 4
495 mm diameter Teflon tube directed at the fly's antennae. A custom-designed solenoid valve
496 controller system was used to redirect the airstream between a blank cartridge and one containing
497 cVA or Ethanol (solvent control). To make odour cartridges, 10 μL of undiluted cVA (Cayman
498 Chemicals, 20 mg/mL) or Ethanol were placed on filter papers, and dried for 3 min to remove

499 solvent before inserted into 15 mL pre-cleaned vials (Sigma-Aldrich).

500 **Imaging data analysis.** All data analysis was performed in MATLAB (MathWorks). ROIs (region
501 of interest) corresponding to individual cell bodies were manually selected and fluorescence signal
502 from the ROIs were smoothed with a moving average (window =5 frames). For volume imaging
503 (Fig. 1a, b and ED Fig. 1), a single focal plane in which we observed the highest $\Delta F/F$ was used
504 for each cell. Normalized $\Delta F/F$ values for each trials were calculated by dividing $\Delta F/F$ by the
505 maximum $\Delta F/F$. The average signal before photostimulation was used as F_0 to calculate the $\Delta F/F$,
506 and cells with peak $\Delta F/F$ responses $< 4\sigma$ above baseline more than 1/3 trials were excluded. Decay
507 constants (τ) were fit to minimize mean-squared error between observed $\Delta F/F$ traces and a five-
508 parameter model of cell responses to optogenetic stimulation. Specifically, the $\Delta F/F$ trace evoked
509 by three consecutive pulses of optogenetic stimulation was fit with a weighted sum of three
510 impulse responses sharing a characteristic rise time τ_R and decay time τ : fit values of τ_R
511 and τ were the same for all three evoked responses, while response amplitudes were fit
512 independently. Fit impulse responses in the model were set to be 30 s apart, following experimental
513 stimulation conditions. The best-fit 80% of cells ($MSE < 2.06$) were used to generate plots of
514 population-average responses. “Percent of peak” in Fig. 5h and ED Fig. 8c were calculated from
515 mean normalized $\Delta F/F$ values between 10-30 s after GtACR1 actuation. cVA responses for Fig. 6h
516 were calculated by subtracting mean GCaMP signal 10 s before cVA presentation from those
517 obtained during cVA presentation (10 s). cVA responses from each cell delivered 30s after P1
518 stimulation were divided by cVA responses without concurrent P1 stimulation (cVA only), to
519 calculate fold change (Fig. 6i). cVA alone or P1+cVA stimulation were delivered in random order
520 following initial selection for P1-responsive pCd neurons. Individual cell responses used in Fig.
521 6g-i were the average of 2-3 trials per cell.

522 **Labeling neurons with Photoactivation after GCaMP imaging.** Photoactivation experiments
523 were performed in vivo using spiral scanning as described above. To perform GCaMP imaging
524 and PA-GFP activation simultaneously, two Chameleon Ultra II Ti:Sapphire lasers (Coherent), one
525 set at 920 nm and the other at 710 nm, are combined using 760 nm long pass filter (Bruker). Cell
526 bodies of pCd neurons were identified by functional imaging using NLS-GCaMP6s, and a three-
527 dimensional region of photoactivation was defined. The defined region of photoactivation was
528 photoactivated by two cycles of spiral scanning (diameter \approx 7.5 μ m, 45.24 ms/repeat, 20 repeats,
529 150 ms inter-repeat-intervals) separated by 20 min interval to allow diffusion of photoactivated
530 PA-GFP molecules to the projections. 20 min after second cycle of the spiral scanning, 3-
531 dimensional images were acquired at 1024 X 1024 pixel resolution. To reduce the fly's movement
532 and residual GCaMP signal, cold saline containing 1mM EDTA was perfused until the end of
533 image acquisition. tdTomato signals and photoactivated PA-GFP signals were imaged
534 simultaneously at 940 nm. Non-PPF1 PA-GFP and NLS-GCaMP basal fluorescence have been
535 masked for clarity and z stack were created (Fig. 1c₃ and c₄) using Fluorender⁵⁹ and Fiji^{60,61}
536 software.

537 **Immunohistochemistry.** Brains from 7-to-10-day-old adult flies were dissected and stained as
538 previously described³⁵. The primary antibody mixture consisted of 1:1000 rabbit anti-GFP
539 (Thermo Fisher Scientific, Cat#A11122), 1:1000 chicken anti-GFP (Aves Lab, Cat#GFP-1010),
540 1:100 mono-clonal (for GRASP experiment, ED Fig. 4j-r) mouse anti-GFP (Sigma-Aldrich,
541 Cat#G6539), 1:1000 rabbit anti-DsRed (Takara Bio, Cat#632496), 1:50 mouse anti-Brochpilot
542 nc82 (Developmental Studies Hybridoma Bank), and 10% normal goat serum (Sigma-Aldrich) in
543 PBST. Secondary antibodies used were 1:1000 goat anti-rabbit-Alexa488 (Thermo Fisher
544 Scientific, Cat#A11008), 1:1000 goat anti-chicken-Alexa488 (Thermo Fisher Scientific,

545 Cat#A11039), 1:1000 goat anti-mouse-Alexa488 (Thermo Fisher Scientific, Cat#A11001), 1:1000
546 goat anti-rabbit-Alexa568 (Thermo Fisher Scientific, Cat#A11011), and 1:1000 goat anti-mouse-
547 Alexa633 (Thermo Fisher Scientific, Cat#A21050).

548 Confocal stacks were obtained with Fluoview FV1000 or FV3000 (Olympus). Fiji^{60,61} and
549 Fluorender⁵⁹ software was used to create z stack images. For brain registration (ED Fig. 4g-i), the
550 two images shown in ED Fig. 4b and d are registered to T1 template brain⁶² using CMTK
551 registration tools⁶³.

552 **Behavioral assay.** Temperature and humidity of the room for behavioral assay was set to 25°C
553 and 55%, respectively. All naturally occurring behavior assays were performed between 2:00pm
554 to 7:00pm. Optogenetically-induced behaviors were not performed at specific times. All the
555 behavior assays except mating assay (ED Fig. 6) were performed in 8-well acrylic chamber (16
556 mm diameter x 10 mm height, modified from ref¹⁵, and side of the each well was coated with
557 aInsect-a-Slip (Bioquip Products). Temperature probe (Vktech) was inserted into one side of the
558 chamber to accurately monitor the chamber temperature. The clear top plates were coated with
559 Sigmacote (Sigma-Aldrich), and the floor of the arenas was composed of clear acrylic covered
560 with food (2.5% (w/v) sucrose and 2.25% (w/v) agarose in apple juice). Flies were introduced into
561 the chambers by gentle aspiration using a mouth pipette, and the chambers were placed under the
562 behavioral setup. Flies were allowed to acclimate to the chamber under the camera without
563 disturbance for 90 s before the recording. Fly behaviors were recorded at 30 Hz using Point Grey
564 Flea3 camera mounted with Fujinon lens (HF35HA-1B) fitted with a long pass IR filter (780 nm,
565 Midwest Optical Systems). Camera was located ~0.5 m above the chamber, and IR backlighting
566 (855 nm, SmartVision Lights) was used for illumination from beneath the arena.

567 Optogenetic activation was performed as described previously¹⁵. Briefly, a 655 nm 10 mm Square

568 LED (Luxeon Star) was used to deliver 0.48 mW/mm^2 light for 30 seconds. For dead female
569 presentation (Fig. 3d-f and j-l, Fig. 4a, and ED Fig. 9), 2-5 day old wild-type Canton S virgin
570 females were freeze-killed, and affixed in the middle of the arena with UV curable glue. The
571 ventral end of the female abdomen was glued to prevent copulation.

572 For the female induced aggression assay (Fig. 6a-d), single-housed male flies were transferred
573 individually into empty vials containing a virgin female, and allowed to freely interact with the
574 female for ~5 min. After this pre-exposure period, the male flies were gently transferred to the
575 behavior arena covered with 2.25% (w/v) agarose in dH₂O, instead of fly food. For GtACR1
576 stimulation (Fig. 6c-d and ED Fig. 9), a 530 nm 10 mm Square LED (Luxeon Star) was used to
577 deliver $117 \mu\text{W/mm}^2$ light for 10 seconds. Male flies that initiated copulation during the 5 min pre-
578 exposure period were not tested.

579 For the mating assay (ED Fig. 6), 12-well two-layer chambers in which the layers were separated
580 by a removable aluminum film. 2-5 day old wild-type Canton S virgin females were introduced
581 into the lower layers, and males of a particular genotype were introduced in the upper layers. Flies
582 were allowed to acclimate to the chamber for 90 s as described above before removing film.
583 Behavior recording started right after film was removed.

584 **Behavioral data analysis.** Analysis of lunging and unilateral wing extension was performed as
585 described in ref⁹. Briefly, fly posture was tracked from recorded videos using Caltech FlyTracker
586 software, which is available for download at <http://www.vision.caltech.edu/Tools/FlyTracker/>, and
587 bouts of behaviors were automatically annotated using the Janelia Automatic Animal Behavior
588 Annotator (JAABA)⁶⁴. All annotations were manually validated to remove false positives.
589 Behavioral assays with dead females (Fig. 3d-f and j-l) were manually scored without using
590 JAABA due to inaccuracy. Data shown in Fig. 3a-c and g-i were also manually scored for

591 consistency. Copulation latency for ED Fig. 6 was manually scored, and the total number of males
592 that had engaged in copulation was summed across the 30-min period and plotted as a percentage
593 of total flies for each time point. Courtship bouts shown in ED Fig. 9 were manually annotated
594 following the definition of courtship bouts described previously¹⁷. Statistical analyses were
595 performed using Matlab and Prism6 (GraphPad Software). All data were analyzed with
596 nonparametric tests. The cutoff for significance was set as an $\alpha < 0.05$. Each experiment was
597 repeated at least twice on independent group of flies. Outliers were defined as data points falling
598 outside 1.5x the interquartile range of the data, and were excluded from plots for clarity, but not
599 from statistical analyses.

600 **Curve Fitting for Leaky bucket model.** Rasters of courtship and lunging behavior in a 15-minute
601 window were averaged across flies and binned in 10-second (for courtship) or 20-second (for
602 lunging) time windows to produce a time-evolving population average behavior rate. Behavior
603 rates for courtship and lunging were each fit with a three-parameter leaky integrator model with
604 dynamics $\dot{r}(t) = -r(t)/\tau + I$, which has analytical solution $r(t) = (r_0 - \tau I)e^{-t/\tau} + \tau I$, where r
605 is the behavior rate as a function of time t (in minutes), I is a constant sensory input, τ is the time
606 constant of integration, and r_0 is the initial behavior rate at the start of recording.

607 Parameters I , τ , and r_0 were fit to minimize the mean squared error between model and data, for
608 courtship and for lunging. Parameter values were jointly fit across the two behaviors (courtship
609 and lunging) and across the four experimental conditions: pCd > Kir2.1 (manipulation), pCd >
610 GFP, BPD > Kir2.1, and BPD > GFP (controls). To reduce the number of free parameters, the
611 sensory input I was constrained to take the same value for all groups and conditions, while r_0 was
612 fit separately for courtship and for aggression; only τ was fit independently for each group and
613 each behavior.

614 **METHODS REFERENCES**

- 615 53 Pfeiffer, B. D. *et al.* in *Proc Natl Acad Sci USA* Vol. 105 9715-9720 (National Acad
616 Sciences, 2008).
- 617 54 Adams, M. D. *et al.* The genome sequence of *Drosophila melanogaster*. *Science* **287**, 2185-
618 2195, (2000).
- 619 55 Pavlou, H. J. *et al.* Neural circuitry coordinating male copulation. *eLife* **5**, (2016).
- 620 56 Lai, S. L. & Lee, T. Genetic mosaic with dual binary transcriptional systems in *Drosophila*.
621 *Nature neuroscience* **9**, 703-709, (2006).
- 622 57 Gordon, M. D. & Scott, K. Motor control in a *Drosophila* taste circuit. *Neuron* **61**, 373-384,
623 (2009).
- 624 58 Hoyer, S. C. *et al.* Octopamine in male aggression of *Drosophila*. *Current biology : CB* **18**,
625 159-167, (2008).
- 626 59 Wan, Y., Otsuna, H., Chien, C. B. & Hansen, C. An interactive visualization tool for multi-
627 channel confocal microscopy data in neurobiology research. *IEEE transactions on*
628 *visualization and computer graphics* **15**, 1489-1496, (2009).
- 629 60 Schindelin, J. *et al.* Fiji: an open-source platform for biological-image analysis. *Nat*
630 *Methods* **9**, 676-682, (2012).
- 631 61 Schneider, C. A., Rasband, W. S. & Eliceiri, K. W. NIH Image to ImageJ: 25 years of image
632 analysis. *Nat Methods* **9**, 671-675, (2012).
- 633 62 Yu, J. Y., Kanai, M. I., Demir, E., Jefferis, G. S. X. E. & Dickson, B. J. Cellular organization
634 of the neural circuit that drives *Drosophila* courtship behavior. *Current biology : CB* **20**,
635 1602-1614, (2010).
- 636 63 Jefferis, G. S. *et al.* Comprehensive maps of *Drosophila* higher olfactory centers: spatially

637 segregated fruit and pheromone representation. *Cell* **128**, 1187-1203, (2007).

638 64 Kabra, M., Robie, A. A., Rivera-Alba, M., Branson, S. & Branson, K. in *Nat Methods* Vol.
639 10 64-67 (2013).

640 65 Baines, R. A., Uhler, J. P., Thompson, A., Sweeney, S. T. & Bate, M. Altered electrical
641 properties in *Drosophila* neurons developing without synaptic transmission. *J Neurosci* **21**,
642 1523-1531, (2001).

643 66 Diao, F. *et al.* Plug-and-play genetic access to *drosophila* cell types using exchangeable
644 exon cassettes. *Cell reports* **10**, 1410-1421, (2015).

645

646

647

648

649

650

651

652

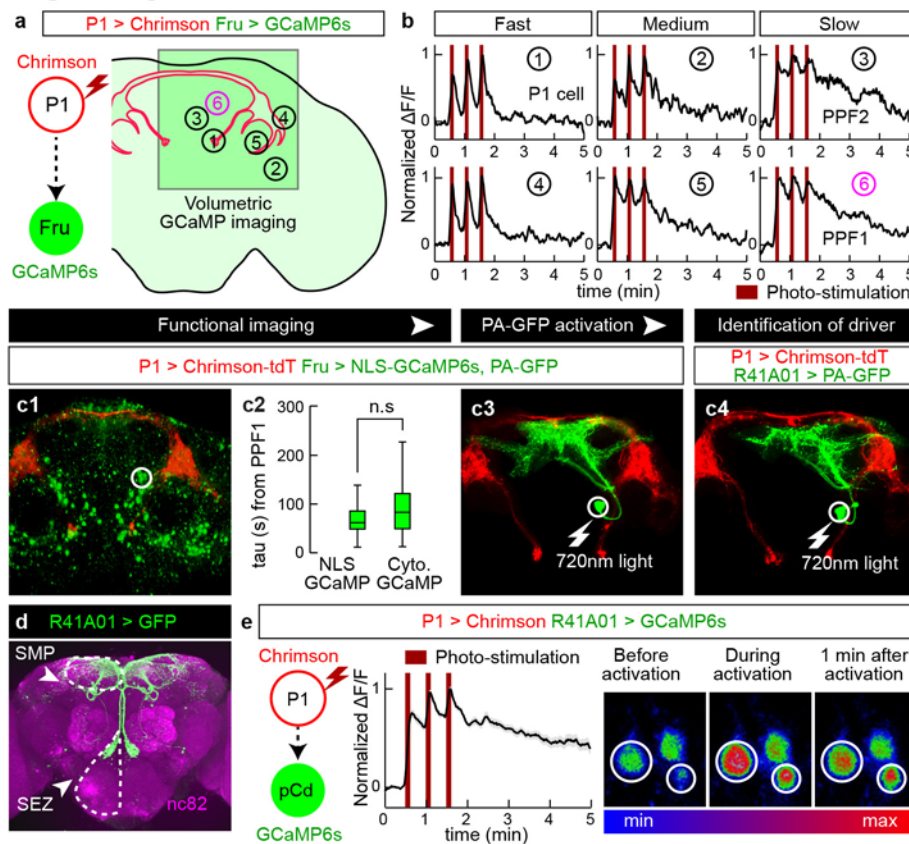
653

654

655

656 **FIGURES**

Jung et al., Fig. 1



657

658 **Figure 1. Identification of P1 follower cells with long-lasting responses.**

659 (a) Experimental schematic. Green square indicates imaging field containing different putative P1
 660 follower cells (numbered circles). (b) Representative GCaMP6s traces (normalized $\Delta F/F$);
 661 numbers correspond to cells in (a). PPF1 cells (⑥) are pCd neurons. 655 nm light (10 Hz, 10 ms
 662 pulse-width, 25 s inter-stimulation interval) was delivered for Chrimson stimulation (dark red bars).
 663 (c₁₋₄) Identification of GAL4 driver labeling PPF1 (pCd) neurons (See ED Fig. 2a for details). (c₁)
 664 LexAop-NLS-GCaMP expressed in Fru-LexA neurons; white circle, PPF1 somata. (c₂)
 665 Comparison between NLS GCaMP6s and Cytoplasmic GCaMP6s. Decay constants (τ) were
 666 calculated by curve fitting (See ED Fig. 1i and Methods for details). n=32 trials, 11 cells from 7

667 flies (NLS GCaMP), 77 cells from 12 flies (Cytoplasmic GCaMP). Statistical significance in this
668 and in all other figures (unless otherwise indicated) was calculated using a Mann-Whitney U-test.
669 Boxplots throughout show the median (center line), 25th and 75th percentiles (box), and 1.5 times
670 the interquartile range (whiskers). Outliers were defined as data points falling outside 1.5x the
671 interquartile range of the data, and were excluded from plots for clarity, but not from statistical
672 analyses. (c₃) PPF1 projections revealed by Fru-LexA>PA-GFP activation²³. (c₄) PPF1 neurons
673 labeled by R41A01-LexA>PA-GFP. Non-PPF1 PA-GFP and NLS-GCaMP basal fluorescence
674 have been masked for clarity. All images in c₁, c₂, and c₄ are maximum intensity z-projections of
675 2- μ m optical sections acquired by 2-P imaging. (d) Central brain R41A01 Gal4 neurons revealed
676 by UAS-myr::GFP reporter. Superior medial protocerebrum (SMP) and sub-esophageal zone
677 (SEZ) are indicated by dashed outlines. (e) LexAop-GCaMP6s response of pCd neurons labeled
678 by R41A01-LexA following P1-Gal4/UAS-Chrimson stimulation (see Supp. Table 1 for
679 genotypes). Left, schematic; middle, normalized $\Delta F/F$ trace (n=23 trials, 15 cells from 10 flies;
680 mean \pm sem); right, fluorescent images taken before, during, and 1 minute after P1 activation
681 (averaged over 5 frames). White circles indicate two responding cells.

682

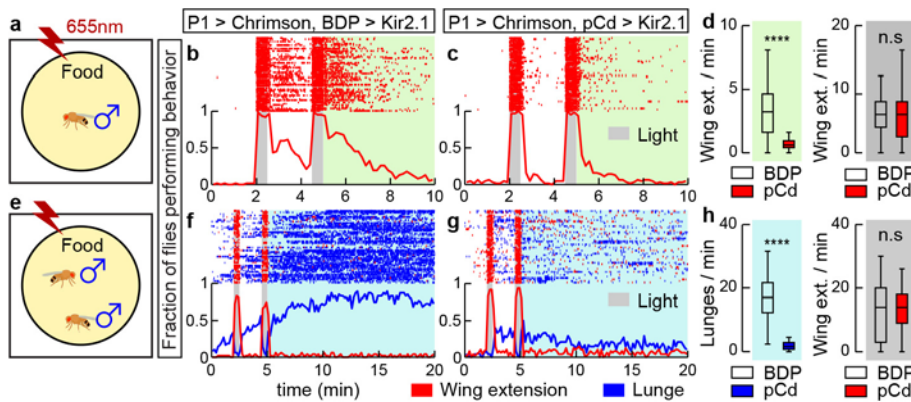
683

684

685

686

Jung et al., Fig. 2

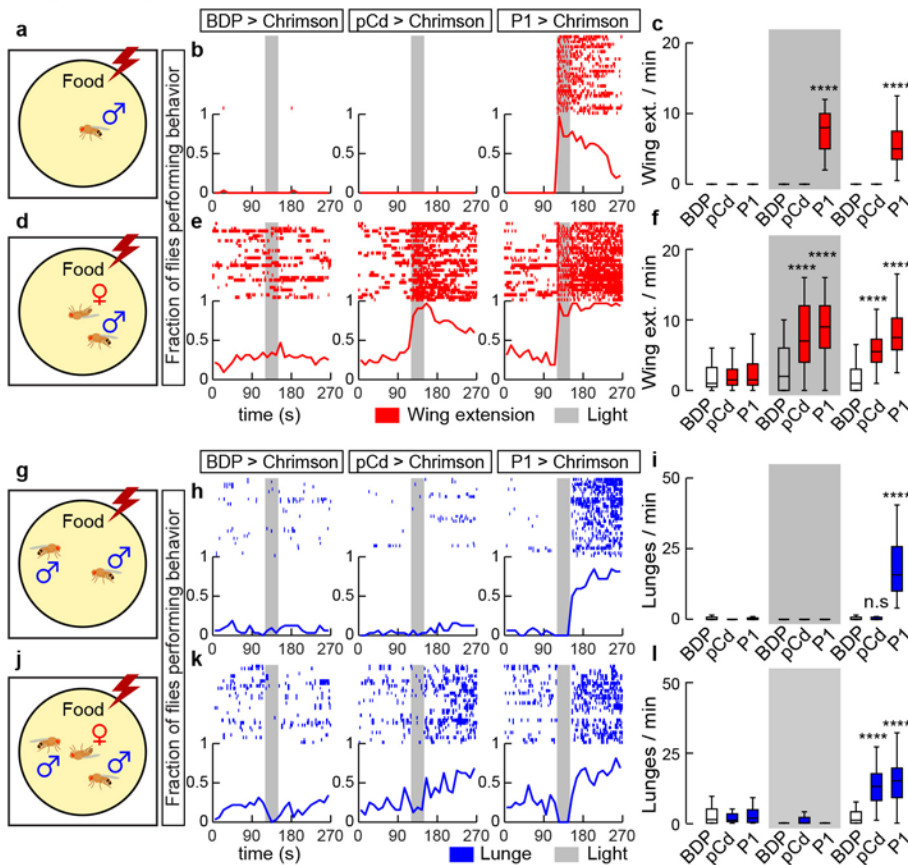


687

688 **Figure 2. Activity of pCd neurons is required for P1-induced persistent behaviors.**

689 (a) Schematic (approximately to scale). Chrimson activation at 655 nm¹⁵ was performed in solitary
690 males on food. (b-c) Behavior of flies during (gray shading) and after (green shading) P1^{a9,20}
691 neuronal activation, either without (b; BDP is enhancerless LexA control driver), or with (c; pCd-
692 LexA) Kir2.1-mediated⁶⁵ inhibition of pCd neurons. Grey bars, 30 s photostimulations (40 Hz, 10
693 ms pulse-width) at 2 min intervals. Upper: Wing extension raster plot (red ticks). Lower: fraction
694 of flies performing wing extensions (red line) in 10 s time bins. n=62 (b), 63 (c). (d) Wing
695 extension frequency per fly after (green shading) or during (grey shading) photostimulation. ****
696 $P < 0.0001$. (e) As in (a), but using male pairs. (f-g) Plot properties as in (b-c). Grey bars, 30 s
697 photostimulation periods (2 Hz, 10 ms pulse-width) at 2 min intervals. Upper: raster plot showing
698 wing extensions (red ticks) and lunges (blue ticks). Lower: fraction of flies performing wing
699 extensions (red line) or lunges (blue line) in 20 s time bins. n=48 for each genotypes. (h) Lunge
700 frequency after photostimulation (light blue shading, left), and wing extension frequency during
701 photostimulation (grey shading, right). Lunging during, and wing extension after photostimulation
702 were ≤ 1 event/min and are omitted for clarity. Statistics as in (d).

Jung et al., Fig. 3

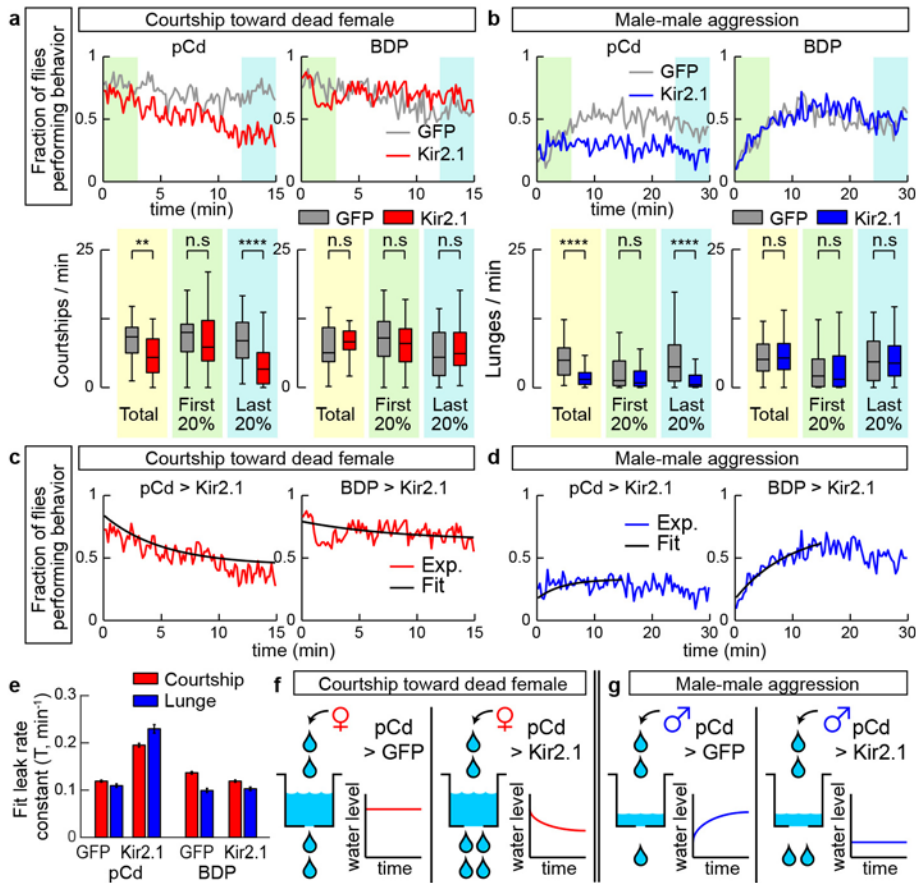


703

704 **Figure 3. Activation of pCd neurons amplifies and extends male social behaviors induced by**
 705 **female cues.**

706 (a, d, g, and h), experimental schematics illustrating optogenetic activation of pCd neurons in
 707 solitary males (a-f) or pairs of group-housed males (g-l), tested without (a-c, g-i) or with (d-f, j-l)
 708 a dead female. Raster plots and fraction of flies performing behaviors (red and blue lines, 10 s time
 709 bins) are shown in (b, e, h, and k). Plot properties same as in Fig. 2. Grey bars, 30 s Chrimson
 710 activation at 655 nm (10 Hz, 10 ms pulse-width). Quantification and statistical tests shown in (c,
 711 f, i, and l). n=32 flies each. Statistical test used was a Kruskal-Wallis test. **** Dunn's corrected
 712 $P < 0.0001$ for between-genotype comparisons. Courtship data are omitted in (h, k) for clarity.

Jung et al., Fig. 4



713

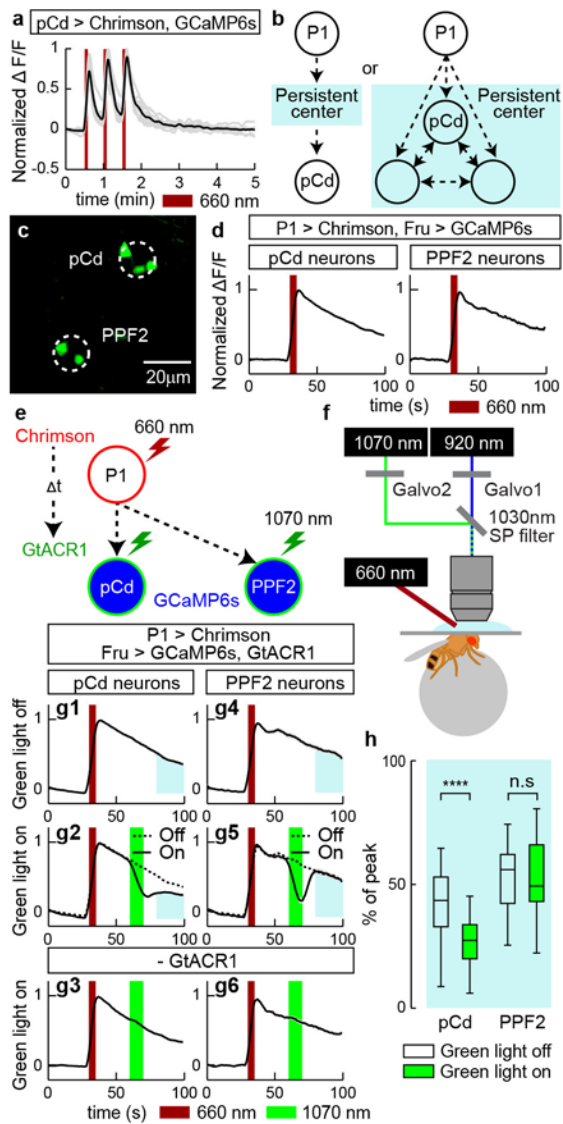
714 **Figure 4. Inhibition of pCd neurons reduces endurance of naturally occurring social**
 715 **behaviors.**

716 (a) Solitary male flies were incubated with a dead female and courtship (unilateral wing extension
 717 bouts, UWEs) measured over 15 min. Left panels show experimental (pCd>Kir2.1, red line) and
 718 responder control (UAS-GFP, grey line) flies, right panels show enhancerless driver controls
 719 (BDP-Gal4; red and grey lines). Upper: fraction of flies performing behavior in 10 s time bins.
 720 Lower: number of UWE bouts per min per fly over entire 15 min observation (yellow shading),
 721 first (green shading) and last (blue shading) 20% (3 min) of the interval. n=40 flies per genotype.
 722 ** $P < 0.01$, **** $P < 0.0001$. (b) Pairs of single-housed males monitored over 30 min. Plot
 723 properties and statistical tests same as in (a), except blue color indicates lunging. Fraction of flies

724 performing behavior was binned in 20 s time intervals. n=64 flies per genotypes. (c-d) Curve fitting
725 of (c) courtship data from (a), or (d) lunging data from (b). Black lines show exponential fit curve
726 for each experiment. Goodness of fit (MSE): courtship; 0.0042 (pCd>GFP), 0.0051 (pCd>Kir2.1),
727 0.0056 (BDP>GFP), 0.0058 (BDP>Kir2.1); Aggression; 0.0028 (pCd>GFP), 0.0031
728 (pCd>Kir2.1), 0.0045 (BDP>GFP), 0.0029 (BDP>Kir2.1). (e) Leak rate constants derived from
729 curve fitting in (c, d); note that both courtship and lunging in pCd>Kir2.1 flies are best fit by
730 assuming increased leak constants, relative to genetic controls. (f, g) Illustration of modeling
731 results. Water level represents level of activity in a hypothetical leaky integrator driving behavior⁴⁰.
732 Inhibition of pCd activity with Kir2.1 increases leak rate constant of the integrator.

733

Jung et al., Fig. 5



734

735 **Figure 5. pCd neuronal activity is required for physiological persistence.**

736 (a) pCd response to direct optogenetic stimulation is not persistent. Gray lines depict individual
 737 pCd cell responses (n=27 from 9 flies), black line shows the mean for all cells. Dark red bars,
 738 Chrimson stimulation (655 nm light (10 Hz, 10 ms pulse-width, 25 s inter-stimulation interval).
 739 (b) Schematic illustrating alternatives tested by the experiment in (e-h). Light blue shading depicts
 740 hypothetical persistence-encoding network (“center”). If pCd neurons simply inherit persistence

741 passively from the center (left), then persistence should rebound following transient pCd silencing.
742 If persistence does not rebound, it implies that pCd activity is required for the center to maintain
743 persistence (right). (c) Representative two-photon image showing cell body locations of pCd and
744 PPF2 neurons expressing *Fruitless>GCaMP6s* in vivo. Dashed white circles indicate spiral
745 scanning area for GtACR actuation in (e-h). Maximum intensity projection of 5 x 4 μm optical
746 sections, averaged over 10 frames. (d) Normalized $\Delta F/F$ traces from pCd (left, n=36 trials from 8
747 flies), and PPF2 (right, n=29 trials from 5 flies) neurons upon P1 activation. Mean \pm sem. Dark red
748 bar indicates P1 photostimulation (5 s, 10 Hz, 10 ms pulse-width, 660 nm LED). (e) Experimental
749 schematic. pCd or PPF2 neuron cell bodies are locally photo-inhibited with GtACR1 (~10 s, spiral
750 scanning, see Methods for details) after a delay (Δt , 25 s) following P1 activation (5 s). (f)
751 Schematic illustrating imaging setup with 1070 nm 2-photon laser for GtACR1 photo-inhibition,
752 and 920 nm 2-photon laser for in vivo GCaMP imaging. (g) Normalized $\Delta F/F$ from pCd neurons
753 (g_1 - g_3), and PPF2 neurons (g_4 - g_6) with GtACR actuation (green bars) applied during P1-induced
754 persistent phase. g_1 and g_4 : without photo-inhibition; g_3 and g_6 , 1070 nm irradiation without
755 GtACR1 expression. Dashed lines in g_2 and g_5 are mean of g_1 and g_4 traces, respectively. n=36
756 trials from 8 flies for pCd neurons, and 16 (5 flies) for PPF2 neurons. n=40 (8 pCd flies), 29 (6
757 PPF2 flies) for genetic controls. Mean \pm sem. (h) Normalized area under the curve (blue shaded
758 regions in (g)) after photo-inhibition. **** $P < 0.0001$.

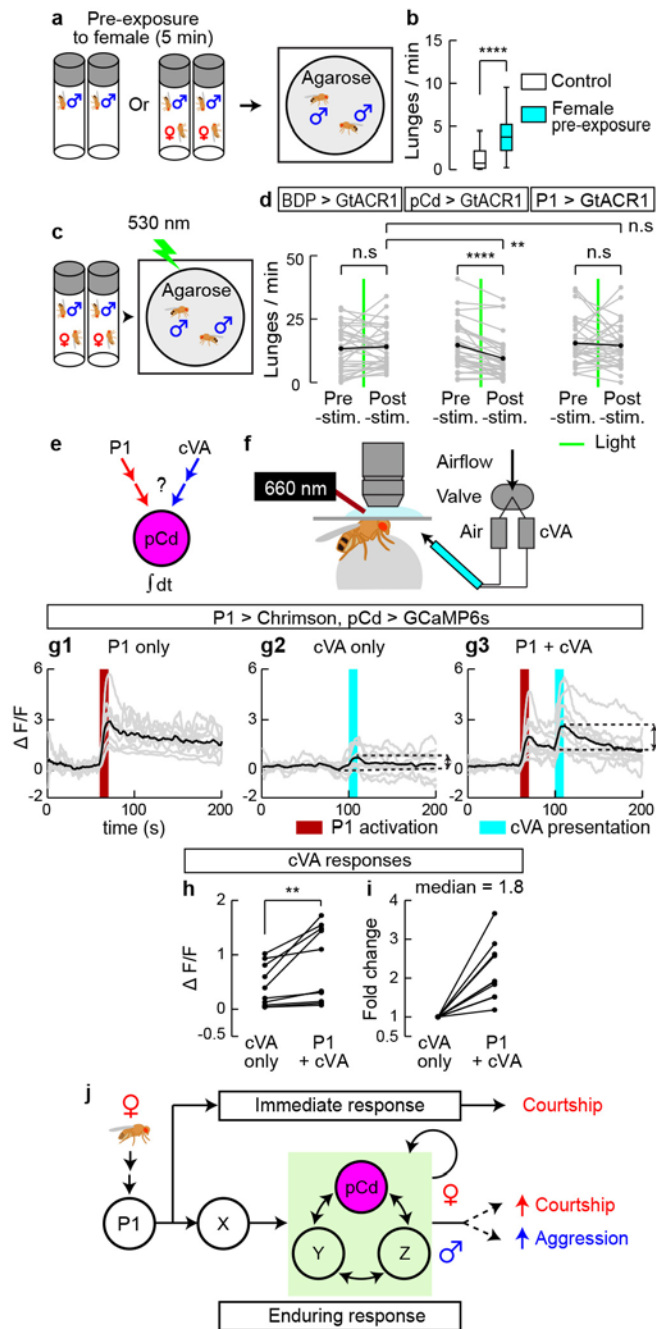
759

760

761

762

Jung et al., Fig. 6



763

764 **Figure 6. Role of pCd neurons in a female-induced enhancement of male aggressiveness.**

765 (a) Schematic illustrating female induced inter-male aggression experiment. Single-housed male

766 flies were pre-incubated in vial with or without (control) a virgin female for 5 min. Subsequently,

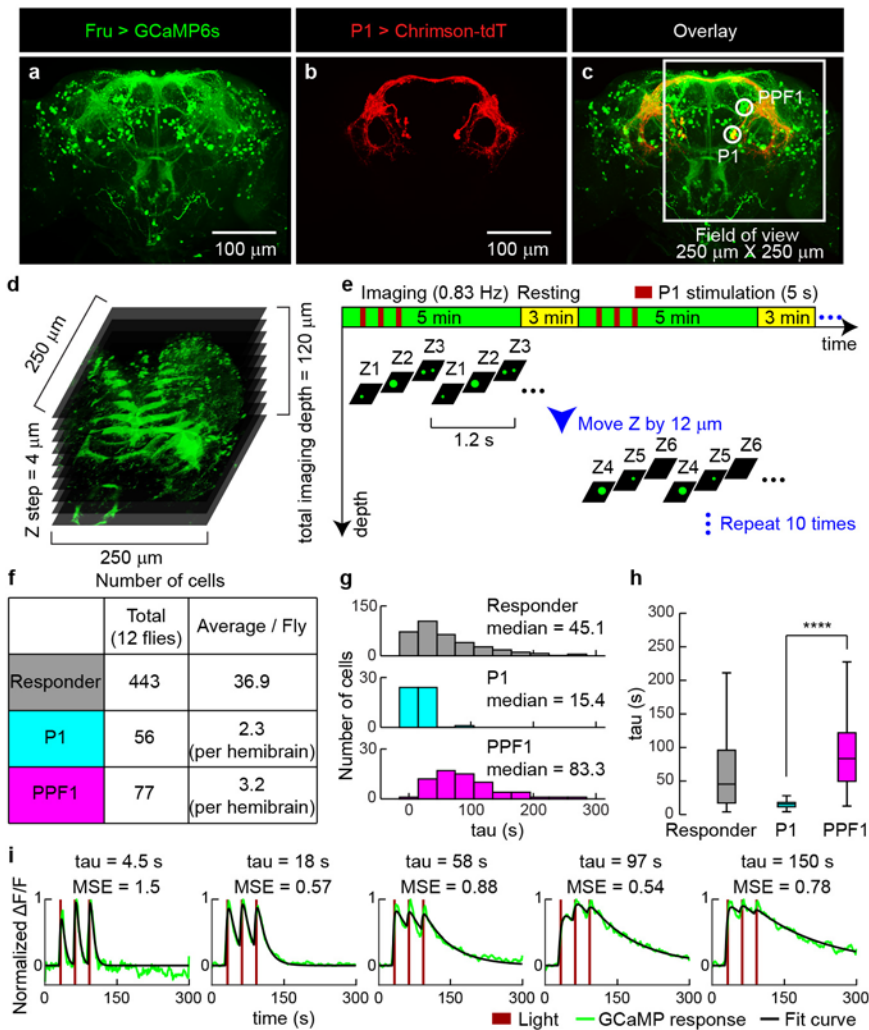
767 pairs of pre-incubated males were placed in behavioral arenas with an agarose substrate. (b) Lunge
768 frequency per fly after pre-incubation without (white) or with (blue) a female. $n=32$ flies each.
769 Statistical test used was a Mann-Whitney U-test. **** $P < 0.001$. (c) Schematic of experimental
770 design. (d) Lunge number before (pre-stim.) and after (post-stim.) GtACR1-mediated neural
771 silencing. Green lines depict exposure to green light (530 nm, 10 Hz, 10 ms pulse-width) for 10 s.
772 Gray points show lunge frequencies for individual flies, and black points show mean values.
773 Statistical tests used were Wilcoxon signed test (within fly comparison) and Kruskal-Wallis test
774 (between genotype comparison). ** Dunn's corrected $P < 0.01$, **** $P < 0.0001$ (e) Schematic
775 illustrating experimental design. (f) In vivo GCaMP imaging. P1 neurons were optogenetically
776 activated (660 nm LED), and cVA (or air) was delivered using an olfactometer synchronized and
777 controlled by the imaging acquisition software. (g) GCaMP responses ($\Delta F/F$) to cVA of pCd
778 neurons exhibiting persistent responses to P1 photostimulation (g_1 , dark red bar, 10 s, 10 Hz, 10
779 ms pulse-width). cVA alone (g_2 , cyan bar) or 30 s after a second (10 s) P1 stimulation (g_3) were
780 delivered 3 min apart in random order (Methods). Gray lines depict trial-averaged individual pCd
781 cell responses (2-3 trials/cell, $n=10$ cells from 7 flies) and black lines show the mean for all cells.
782 Double-headed arrows in (g_2 and g_3) indicate intervals for cVA responses calculated in (h-i). (h)
783 Individual pCd cell responses ($\Delta F/F$) to cVA presented alone ("cVA only") or 30 s after a 10 s P1
784 stimulation ("P1+cVA"). Statistical test used was a Wilcoxon signed-rank test. ** $P < 0.01$. (i)
785 Fold change of pCd responses to cVA presentation after P1 stimulation, compared to cVA
786 delivered alone. Data normalized to $\Delta F/F$ without P1 stimulation. (j) Models for how P1 and pCd
787 neurons regulate immediate and enduring social behaviors.

788

789

790 **EXTENDED DATA FIGURES**

Jung et al., ED Fig. 1



791

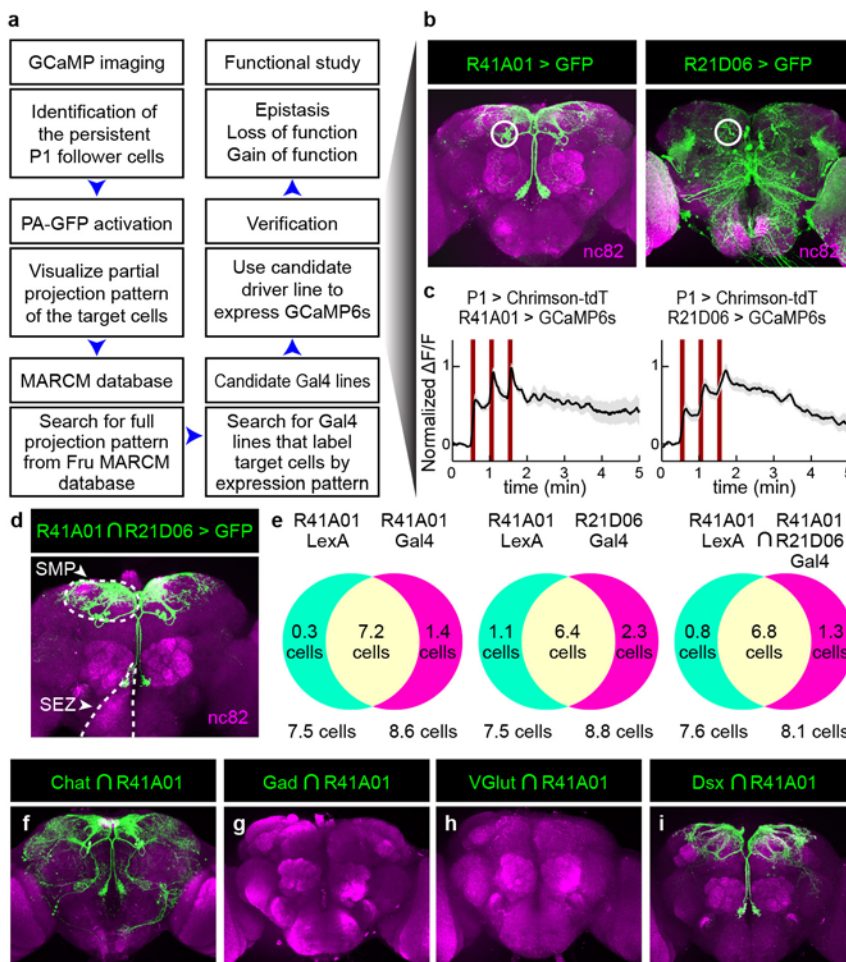
792 **Extended Data Figure 1. Volumetric functional GCaMP imaging to identify persistent P1**
 793 **follower cells.**

794 (a-c) Maximum intensity confocal stacks showing projection patterns of Fruitless (a) and P1^a (b)
 795 neurons^{9,20} expressing GCaMP6s and Chrimson-tdT, respectively; (c), overlay. (d-e) Schematics
 796 illustrating functional connectomics strategy. Responses to P1^a photostimulation (3 x 5 s pulses)
 797 from multiple Fru>GCaMP6s cells in each imaging plane (250 x 250 μm²) were recorded during

798 ten 5 min trials, at multiple z-depths (4 $\mu\text{m}/\text{z-step}$) covering 120 μm . (f) Number of Fruitless⁺ cells
799 that responded to P1^a activation. PPF1 cells were identified anatomically in high-resolution images
800 acquired following P1 stimulation trials, using 40 mM KCl-containing saline to increase baseline
801 GCaMP6s signals. Red channel (Chrimson-tdTomato) was used to identify P1 neurons, and cell
802 body position and primary projection pattern were used to identify PPF1 neurons. P1 and PPF1
803 were visible in both hemi-brains of all specimens, but some responder cells on the lateral side
804 appeared only in one hemi-brain (see Field of view marked in (c)). (g) Histogram of τ (tau, decay
805 constant of a model exponential fit to observed neural $\Delta F/F$ traces) for all responder cells (top,
806 grey), P1 cells (middle, light blue), and PPF1 neurons (bottom, magenta). (h) Quantification and
807 statistical test for τ . Statistical test used was a Mann-Whitney U-test. **** $P < 0.0001$. τ from 80%
808 of the total identified cells (MSE ≤ 2.06 , 354 cells) were used for the plot (g) and quantification
809 and statistical test (h). (i) Representative examples of GCaMP responses and τ for different
810 responder cells. Dark red lines indicate Chrimson activation at 660 nm (3 stimulations, 5 s each,
811 10 Hz, 10 ms pulse-width, 25 s inter-stimulation interval).

812

Jung et al., ED Fig. 2



813

814 **Extended Data Figure 2. Gaining genetic access to PPF1 neurons and molecular phenotype**
 815 **of pCd neurons.**

816 (a) Flowchart of the protocol for identifying specific Gal4 lines labeling PPF1 neurons. (b)
 817 Anatomy of two Gal4 lines, R41A01 (left) and R21D06 (right) that label PPF1 neurons.
 818 Maximum-intensity projection (z-stack) of confocal 2- μ m optical sections. (c) Functional imaging
 819 of putative PPF1 neuronal cell bodies labeled by R41A01-LexA (left) and R21D06-LexA (right).
 820 Traces represent normalized $\Delta F/F$ response to P1 stimulation (dark red bars, 3 repeats of 5 s
 821 stimulation, 10 Hz, 10 ms pulse-width, 25 s inter-stimulation interval), and were obtained from
 822 cell bodies within the white circles indicated in (b). Mean \pm sem, n=7 (4 flies) for R41A01, and 9

823 (4 flies) for R21D06. (d) Anatomy of split-Gal4 intersection between R41A01-AD and R21D06-
824 DBD in the male brain. SMP and SEZ are indicated with white dashed line. (e) Quantification of
825 pCd cell numbers (per hemibrain) labeled by two different reporters, UAS>tdTomato and
826 LexAop>GFP, in flies co-expressing the indicated GAL4 or LexA drivers. Green=GFP positive,
827 Red=tdTomato positive, Yellow=double positive. Area of Venn diagram not scaled to number of
828 cells. n=12 hemibrains per test. (f-i) Anatomy of split intersection between R41A01-AD and Chat-
829 DBD⁶⁶ (f), Gad1-AD and R41A01-DBD (g), R41A01-AD and VGlut-DBD (h), and R41A01-AD
830 and dsx-DBD. Maximum-intensity projection of confocal 2- μ m optical sections.

831

832

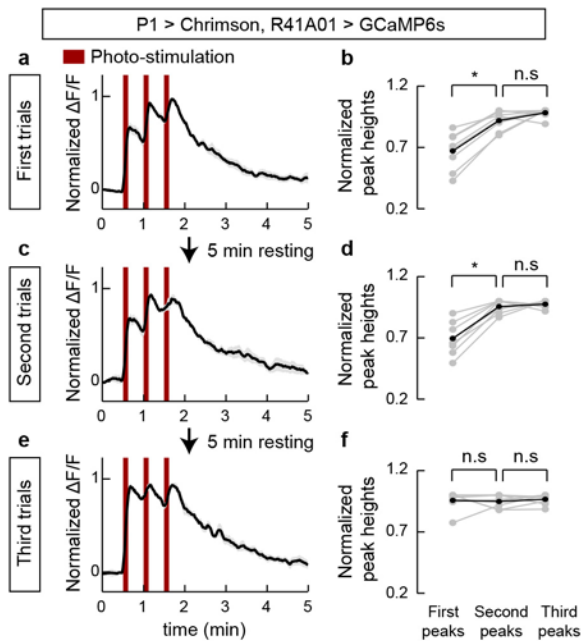
833

834

835

836

Jung et al., ED Fig. 3



837

838 **Extended data Figure 3. Integration of repeated P1 input by pCd neurons.**

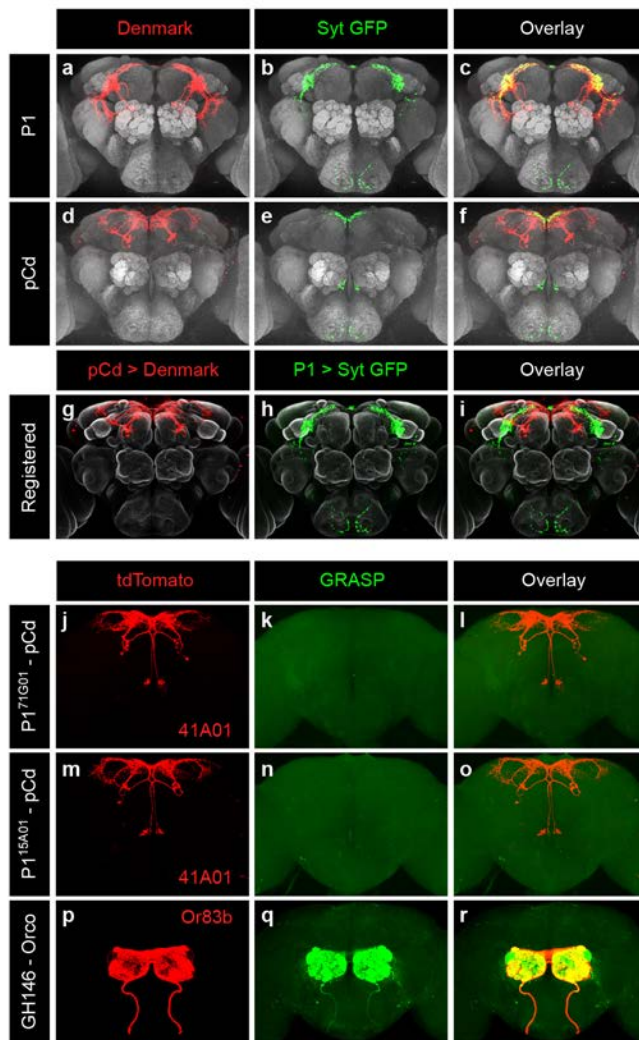
839 (a, c, e) Normalized GCaMP response of pCd neurons to optogenetic stimulation of P1 neurons.

840 Mean \pm sem. n=8 cells, 6 flies. (b, d, f) Normalized peak heights during each P1 stimulation.

841 Statistical test used was Wilcoxon signed test with correction for multiple comparisons. * $P < 0.05$

842

Jung et al., ED Fig. 4



843

844 **Extended Data Figure 4. Anatomic relationship between P1 and pCd neurons**

845 (a-f) Input and output region of the P1 and pCd neurons visualized by double-labeling with
846 somatodendritic marker (Denmark, red) and pre-synaptic marker (Syt-GFP, green). (g-i). Co-
847 registered images showing somatodendritic region of pCd neurons and pre-synaptic region of P1
848 neurons. Note that yellow regions in (i, “Overlay”) are not observed when the image is rotated and
849 viewed from a different angle, indicating a lack of overlap. (j-r) GRASP³⁴ experiments performed
850 between R41A01 (pCd driver) and either of two P1 drivers, 71G01 (j-l) and 15A01 (m-o), or

851 between GH146 and Orco as a positive control (p-r). tdTomato was expressed in one of the putative
852 synaptic partners, R41A01 (j and m) or Orco (p), to mark fibers for detailed analysis. No positive
853 GRASP signal is observed between pCd and either of the 2 P1 drivers (j-o).

854

855

856

857

858

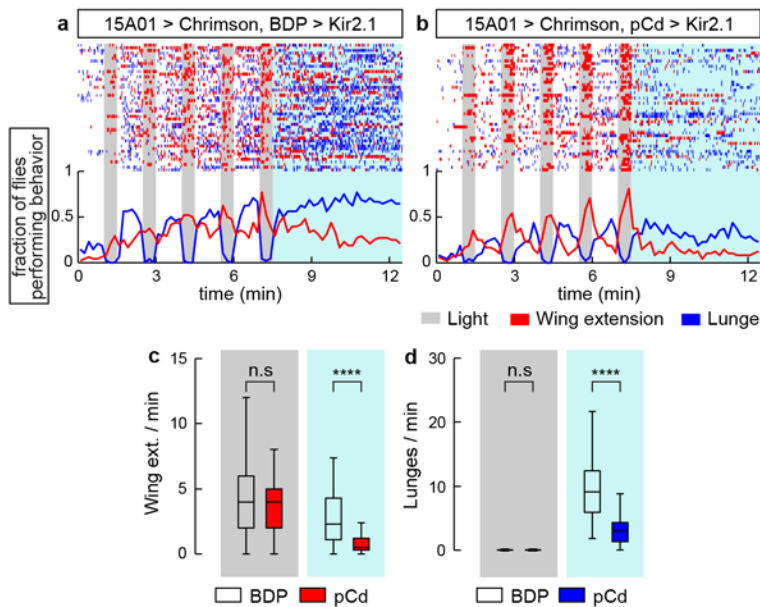
859

860

861

862

Jung et al., ED Fig. 5



863

864 **Extended Data Figure 5. Inhibition of pCd neurons with R41A01∩R21D06 Split-Gal4**
865 **reduces P1-induced social behaviors.**

866 (a-b) Top: raster plot showing wing extensions (red ticks), and lunges (blue ticks) in pair of males.
867 In this experiment, a single driver 15A01-LexA^{9,35} was used to activate P1 neurons, while a split
868 GAL4 driver (ED Fig. 2d) was used to inhibit pCd neurons, complementing the genetic strategy
869 used in Fig. 2 in which a split-Gal4 was used to activate P1 neurons, while R41A01-LexA was
870 used to inhibit pCd neurons (see Table 1 for genotypes). Bottom: fraction of flies performing
871 unilateral wing extensions (red lines), and lunges (blue lines) in 10 s time bins. Gray bars indicate
872 Chrimson activation (5 repeats of 30 s stimulation, continuous light, 60 s inter-stimulation interval).
873 n= 48 flies per genotype. (c-d) Quantification and statistical tests for unilateral wing extensions (c)
874 and lunges (d) during P1 stimulation (gray shading) and after photostimulation (blue shading),
875 without (open boxes, BDP) or with (red boxes) silencing of pCd neurons using Kir2.1 . **** P <

876 0.0001 for between-genotype comparisons (Mann-Whitney U-test). Note that both wing-
877 extensions and aggression are suppressed by pCd silencing during the post-P1 stimulation period.

878

879

880

881

882

883

884

885

886

887

888

889

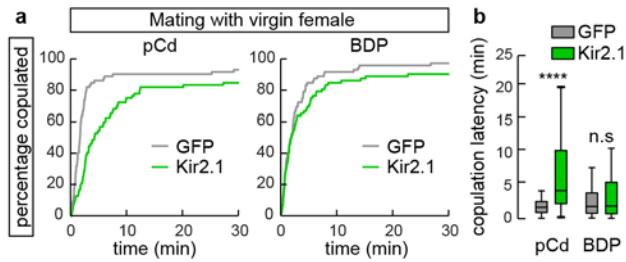
890

891

892

893

Jung et al., ED Fig. 6



894

895 **Extended Data Figure 6. Inhibition of pCd neurons increases copulation latency.**

896 (a) Individual males of the indicated genotypes were paired with a live wild-type virgin female.
897 Cumulative percentage of flies that copulated over 30 min is shown. (b) Quantification and
898 statistical tests for copulation latency. **** $P < 0.0001$ for between-genotype comparisons (Mann-
899 Whitney U-test).

900

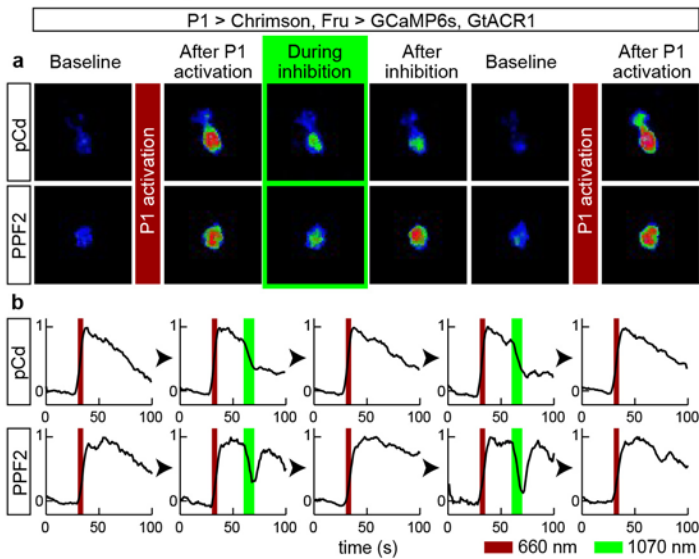
901

902

903

904

Jung et al., ED Fig. 7



905

906 **Extended Data Figure 7. Multiple cycles of P1 stimulation and GtACR1 actuation in pCd**
907 **and PPF2 neurons.**

908 (a) Representative GCaMP fluorescent images of pCd (*upper*) and PPF2 neurons (*lower*) at
909 different time points following Chrimson-mediated P1 stimulation (wide-field LED actuation at
910 660 nm), and cell-restricted GtACR-mediated pCd or PPF2 inhibition (2-photon spiral scanning
911 actuation at 1070 nm). pCd and PPF2 neurons both respond to P1 stimulation, and their response
912 endures following offset of P1 photostimulation (“After P1 activation”). GCaMP signals in pCd
913 neurons rapidly decrease upon photo-inhibition (“During inhibition”, green outline), and do not
914 recover 10 s following offset of GtACR actuation (“After inhibition”). In contrast, PPF2 activity
915 recovers after photo-inhibition. pCd and PPF2 neurons were reliably reactivated by a second cycle
916 of P1 stimulation after following GtACR-mediated inhibition. Images shown are averaged over 5
917 frames. (b) Representative GCaMP trace (normalized $\Delta F/F$) from individual trials. Multiple cycles
918 of P1 stimulation with or without GtACR1 actuation did not change the initial responses of pCd
919 and PPF2 neurons to P1 stimulation. Dark red bar indicates Chrimson activation at 660 nm (5 s,

920 10 Hz, 10 ms pulse-width), and green bar indicates GtACR1 actuation (~10 s, spiral scanning) 25
921 s after Chrimson activation.

922

923

924

925

926

927

928

929

930

931

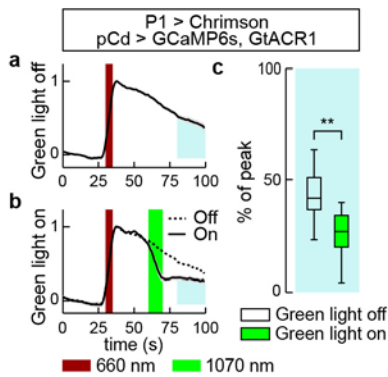
932

933

934

935

Jung et al., ED Fig. 8



936

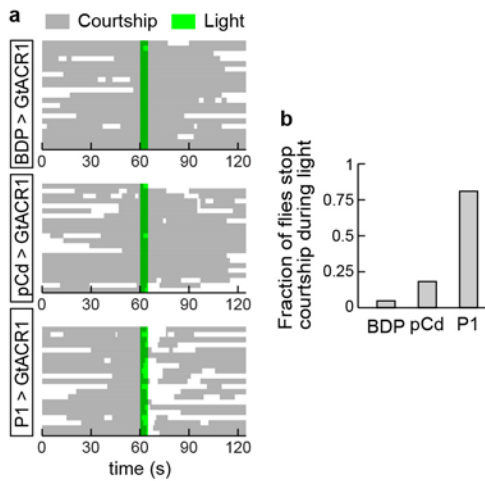
937 **Extended Data Figure 8. GtACR-mediated inhibition of pCd neurons following P1**
938 **stimulation labeled by a pCd-specific driver.**

939 (a) GCaMP6s response of pCd neurons (normalized $\Delta F/F$) labeled with the driver R41A01-LexA
940 (pCd^{R41A01}) to P1 stimulation (dark red bar) without GtACR1 actuation. (b) GCaMP6s response of
941 pCd^{R41A01} to P1 stimulation with GtACR1 actuation. n=10 trials from 3 flies (a-b). Dark red bar
942 indicates Chrimson activation at 660 nm (5 s, 10 Hz, 10 ms pulse-width), and green bar indicates
943 GtACR1 actuation (~10 s, spiral scanning) 25 s after Chrimson activation. (c) Normalized area
944 under the curve after photo-inhibition (blue shaded area in (a-b)). Statistical test used was a Mann-
945 Whitney U-test. ** $P < 0.01$. This experiment confirms the result reported in Fig. 6, in which Fru-
946 LexA was used to express GCaMP6s and pCd neurons were identified morphologically

947

948

Jung et al., ED Fig. 9



949

950 **Extended Data Figure 9. Transient inhibition of P1 neurons interrupt ongoing courtship**
951 **behavior toward dead female.**

952 (a) Raster plot showing courtship toward dead female (gray). Note that “courtship” metric used
953 here incorporates multiple behavioral actions, following the definition used by Zhang et al.¹⁷, and
954 thereby differs from the wing extension metric used in other figures (see Methods for details).
955 Green line indicates GtACR1 stimulation (530 nm, 10 Hz, 10 ms pulse-width) for 10 s. n=21 for
956 BDP and P1 > GtACR1, and 22 for pCd > GtACR1. (b) Fraction of flies stop on-going courtship
957 behaviors during light stimulation.

958